Bulletin of the Seismological Society of America, Vol. 92, No. 5, pp. 1855–1877, June 2002

Comparison of the Taiwan Chi-Chi Earthquake Strong-Motion Data and Ground-Motion Assessment Based on Spectral Model from Smaller Earthquakes in Taiwan

by Vladimir Yu. Sokolov, Chin-Hsiung Loh, and Kuo-Liang Wen

Abstract The design of buildings and structures in earthquake-prone regions must be based on information relating to expected seismic effect. Estimations of time domain and spectral parameters of ground motion are obtained by empirical relations that connect these to earthquake magnitude, distance, and local soil conditions. In the Taiwan region, the models for estimating ground motion parameters were obtained recently on the basis of recordings of small to moderate ($5.0 \leq M_L \leq 6.5$) earthquakes. A large collection of acceleration records from the recent M_L 7.3 (M_w 7.6) Chi-Chi earthquake and aftershocks makes it possible to test the applicability of the established models in the case of larger events. We compared modeled Fourier amplitude spectra and peak accelerations and response spectra, which were calculated using the stochastic approach from the Fourier spectra, and the data obtained during the mainshock and the largest aftershocks (M_L 6.6–6.8). It has been shown that the previously established regional spectral model (Fourier spectra of ground acceleration) may be applied for evaluation of ground motion parameters for earthquakes (reverse faulting) of magnitudes up to M_L 6.8–7.0 and hypocentral depth more than 10 km. To satisfy to the peculiarities of ground-motion propagation during shallow (depth less than 10 km) events, the model should be revised. The analysis of accelerograms from the mainshock (M_L 7.3, depth 8 km, 314 records) and large shallow aftershock (M_L 6.8, depth 10 km, 350 records) allows the authors to obtain the revised spectral model for average-soil conditions.

Introduction

Procedures of seismic hazard assessment are based on ground-motion attenuation relationships, which can be derived from statistical analyses of recorded ground motions or, in conditions of limited strong-motion records, can be obtained from the available literature sources. Ideally, these attenuation models should consider regional earthquake source and propagation path effects and local site response peculiarities. At present, there is no doubt that the relationships are different for different seismic regions, and region-specific and site-specific models should be developed. The empirical databases, however, usually consist of recordings obtained during events of small and moderate magnitudes. A question therefore arises—is it possible to use these relationships in the case of larger events? An important criterion for any simulation procedure is its validation against recorded ground motion. Every strong earthquake provides an unique opportunity to verify the accepted attenuation models and to update empirical relationships. A large collection of recordings from the recent Chi-Chi M_L 7.3 (M_w 7.6) earthquake makes it possible to test the applicability of the recent empirical relationships in the case of a larger earthquake. The distribution of peak ground acceleration and velocities versus distance, as well as the response spectra, for the mainshock were analyzed in several studies (EERI, 1999; Chang et al., 2000; Huang and Chen, 2000; Loh et al., 2000; Tsai and Huang, 2000; Wang *et al.*, 2000). In this article, we consider mainly Fourier amplitude spectra of ground acceleration during the Chi-Chi earthquake mainshock and largest aftershocks.

In recent years, Fourier amplitude spectrum (FAS) is widely used for prediction of ground motion parameters (e.g., Boore and Atkinson, 1987; Atkinson and Boore, 1995; see also Lam *et al.*, 2000, for a review) on the basis of random vibration theory (Hanks and McGuire, 1981; Boore, 1983). The FAS approach also allows estimating seismic intensity in terms of the macroseismic (MMI or MSK) scales (Sokolov and Chernov, 1998; Sokolov, 2000b). Probabilistic seismic hazard analysis based on FAS makes it possible to evaluate so-called site and region and return period–specific strong ground-motion parameters (Sokolov, 2000a; Sokolov

and Chernov, 2001; Sokolov *et al.*, 2001b). Empirical FAS models for estimating design input ground motion parameters in the Taiwan region have been obtained before the Chi-Chi earthquake on the basis of the recordings of small and moderate earthquakes ($5.0 < M_L < 6.5$; 1380 accelerograms) (Sokolov *et al.*, 1999, 2000). It has been shown that the stochastic calculation technique based on these spectral models allows for a satisfactory prediction of the peak ground acceleration and response spectra for distances up to about 200 km in the region (Sokolov *et al.*, 2001a). The goal of this article is to compare Fourier amplitude spectra, peak accelerations, and response spectra modeled for average-soil condition using the models developed for the Taiwan region and the data obtained during the Chi-Chi earthquake and the largest aftershocks. First, we estimated the Fourier acceleration spectra for magnitudes $6.5 \leq M_L \leq 7.5$ on the basis of the recently developed model. The modeled spectra were compared with the observed data for various distances and directions from the earthquake sources. The comparison allowed us to test the existing models and approaches, and to update the models on the basis of new empirical data. Second, the values of effective duration were calculated from accelerograms for every earthquake considered, and a stochastic approach was used for evaluation of peak ground acceleration on the basis of modeled spectra and effective duration. Finally, the response spectra were calculated from the modeled accelerograms for various distances and the modeled spectra were compared with the observed data. The study allows us to conclude that the recently established regional empirical models for Fourier amplitude spectra, which are used for calculation of peak ground acceleration (PGA) and response spectra by a stochastic approach, may be applied to prediction of ground-motion parameters for large earthquakes in the Taiwan region. The models should, however, be revised to satisfy the peculiarities of ground-motion excitation and propagation during shallow earthquakes (hypocentral depth less than 10 km).

Empirical Spectral Model for the Taiwan Region

The model considered in this study is represented by the empirical spectra of ground acceleration estimated for reference distance $R = 1$ km (Fig. 1a, solid lines). These empirical spectra were obtained on the basis of acceleration records in the Taiwan region for magnitude ranges $5.0 < M_L < 5.5$, $5.5 < M_L < 6.0$, and $6.0 < M_L < 6.5$ (Sokolov *et al.*, 1999, 2000). The most significant part of the records, starting from *S*-wave arrival, was analyzed. The records were obtained on various types of soil: from rock sites (class B) to to soft soils (class E) of different thickness (see Lee *et al.*, 2001, for description of site classification). Therefore, averaging the variety of site conditions, the spectral model corresponds to the so-called average soil. Answering the question what does the "average soil" really mean, we assume that the "generic soil" class used by Boore and Joyner (1997) seems to be the most appropriate analogue by means

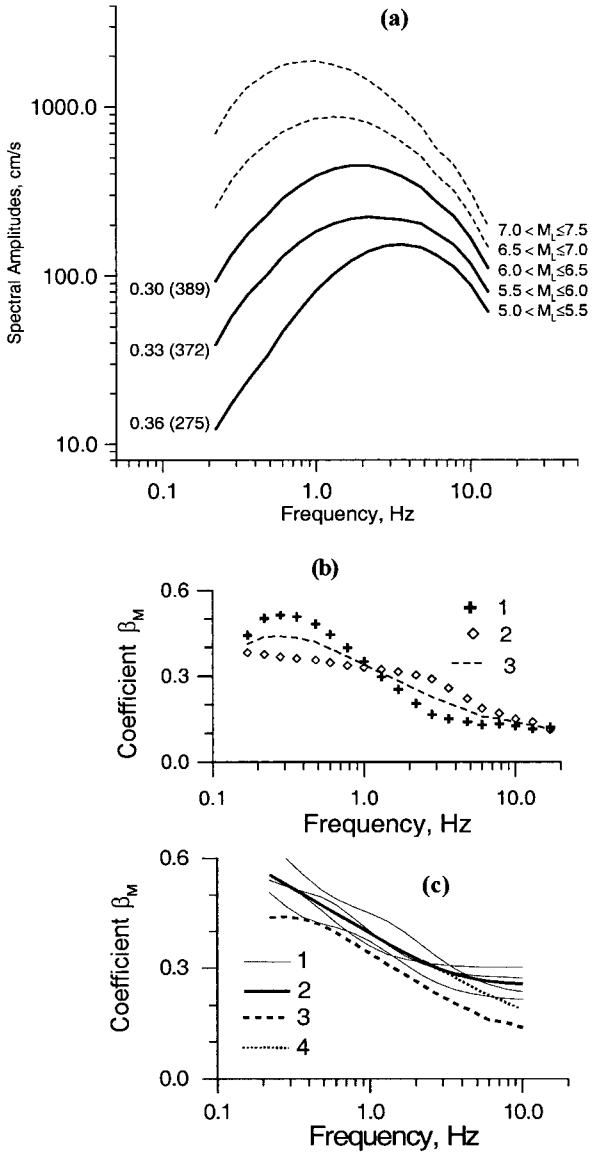

Figure 1. Spectral model for the Taiwan region. (a) Empirical average-soil spectra, reference distance 1 km (solid line). Numbers near the curves denote standard deviation and number of the used records (in parentheses). Dashed lines show the spectra estimated using the coefficients β_M. (b) Frequency dependence of the coefficients β_M (see text) calculated using empirical average-soil spectra for different magnitude ranges (1: $5.5 < M_L < 6.0$ versus $5.0 < M_L < 5.5$; 2: $6.0 < M_L < 6.5$ versus $5.5 < M_L < 6.0$; 3: averaged values). (c) Comparison of frequency dependence of the coefficients β_M that were determined using the two-corner-frequency model (Atkinson and Silva, 2000) for magnitude range $5.5 < M_L < 7.0$ (1, curves for various magnitudes; 2, averaged curve; 3, averaged curve from empirical line; 4, averaged curve for variant of magnitude-dependent kappa-factors [see text]).

of amplification amplitude. On the other hand, the average-soil class, reflecting response of different typical soil classes, should be characterized by a broadband amplification.

The spectrum at a given distance R is calculated by multiplication of the reference distance spectra from a proper magnitude range by

$$R^{b}\exp[-\pi fR/Q(f)V_s], \quad (1)$$

where $b = -1.0$ for distances $R < 50$ km and $b = 0.0$ for $50 < R < 150$–170 km; V_S is the shear wave velocity in the Earth's crust (3.6 km/sec); $Q(f) = 225\,f^{1.1}$ for deep (depth more than 35 km) earthquakes and $Q(f) = 125\,f^{0.8}$ for shallow earthquakes. The trilinear relationship for the geometric attenuation factor R^b is widely accepted (e.g., Atkinson and Silva, 1997, 2000; Lam *et al.*, 2000); however, the characteristic distances R and values of exponent b may differ in various regions.

To extend the model for larger magnitudes, the logarithmic increments (β_M) of spectral amplitudes (A) per unit of magnitude were calculated for frequencies 0.2–12 Hz in the following form,

$$\beta_M(f) = \Delta\log A(f)/\Delta M, \quad (2)$$

where ΔM is the increment of magnitude between the above mentioned magnitude ranges, and A (f) is the reference-distance spectral amplitude (mean values, Fig. 1a). The approach was suggested by Khalturin *et al.* (1975) and further developed by Chernov (1984, 1989). In general, the relation β_M (f) can be represented by

$$\beta_M(f) = c + c_1\log f. \quad (3)$$

The coefficients β_M increase with decreasing of frequency. In other words, as the source energy increases, the intensity of low-frequency vibrations increases more rapidly than that of high-frequency vibrations. Note that this approach allows evaluating ground-motion spectra for large earthquakes on the basis of aftershocks and the smaller events occurred in the study region and it takes into account the focal mechanism effect on seismic radiation excitation. It has been shown (Chernov, 1989) that average β_M (f) relations in the near-field zone for thrust earthquakes (San Fernando, California, 1971; Gazli, Central Asia, 1976 and 1984; Tashkent, Central Asia, 1980; Friuli, Italy, 1976) exhibit a different character compared to those for the strike-slip earthquakes (western United States events; Dagestan, Caucasus, 1971). The thrust earthquakes are characterized by more rapid increase of low-frequency radiation with increase of magnitude than the strike-slip events. The approach was also applied for evaluation of ground acceleration spectra for strong earthquakes in the Caucasus region (Sokolov, 1998) on the basis of earthquakes in the Spitak (Armenia, complex reverse and strike-slip faulting) and Ratchi (northern Georgia, reverse faulting) areas. On the one hand, our spectral model is based on earthquakes of relatively small and moderate earthquakes ($5.0 < M_L < 6.5$); on the other hand, a large amount of ground-motion data from larger earthquakes in the region was obtained. Thus, the comparison of the modeled and empirical data may be considered as verification of the approach.

Figure 1b shows the values β_M that were determined using the empirical average-soil spectra for the Taiwan region ($5.0 < M_L < 6.5$). It has been recently shown on the basis of ω^{-2} source model (Fukushima, 1996) that the scaling law of spectrum amplitude should be considered in the form of a quadratic function of the magnitude within the magnitude range 3.0–8.0. For the case of local magnitude M_L, however, the increase of spectral amplitudes with the increase of magnitude may be accepted as linear (Fukushima, 1996, Fig. 9) for magnitude range 5.0–7.0. We made a comparison of coefficients β_M, which were evaluated on the basis of empirical data and using various spectral models, namely: single-corner-frequency Brune's model and two-corner-frequency models proposed for eastern North America (Atkinson, 1993) and for California (Atkinson and Silva, 2000). These models are based on seismic moment (M_0) values, and we used the M_0/M_L relation given in Figure 8 of Fukushima (1996). For the case of single-corner model, the constant and increasing with magnitude stress parameters were considered. The modeled spectra were calculated for distance 1 km. It has been found (Fig. 1c) that, within magnitude range $5.0 < M_L < 7.0$, the frequency-dependent increments of spectral amplitudes with magnitude that were evaluated from two-corner Californian spectral model exhibit, in general, a good agreement with the empirical Taiwan data. When calculating the modeled spectra, high-frequency amplitudes are reduced using the so-called kappa operator (Anderson and Hough, 1984) by multiplying the spectrum by the factor $\exp(-\pi f\kappa)$. The kappa-filter was introduced to consider near-surface (upper crust) attenuation of seismic waves, and the values of kappa exhibit both a region- and a site-dependent character. When using the same value of kappa for all magnitudes considered, the modeled coefficients β_M (f) become almost independent on frequency for $f > 5$–6 Hz (Fig. 1c); however, it has been shown recently (e.g., Atkinson and Silva, 1997) that the parameter kappa should be also considered a magnitude-dependent quantity. In this case, when values of kappa vary from 0.05 for magnitude 5.0 to 0.065 for magnitude 7.0, the coefficients β_M decrease with increasing frequency, showing better agreement with empirical values.

The absolute values of coefficients β_M depend on the ratio between spectral amplitudes. For the case of the two-corner-frequency model, the coefficients β_M depend also on the ratio between the accepted seismic moment values. Therefore, the higher values of modeled coefficients as compared with the empirical data may be reduced by lowering the corresponding seismic moment values. It seems to be possible to verify the M_0/M_L relation or to construct a regional ω^{-2} source model by comparisons between empirical

Table 1
Parameters of the Chi-Chi Earthquake Mainshock and Aftershocks, Recordings of Which Are Used in This Study

Earthquake code	Date and time (UT)	Latitude, N	Longitude, E	Depth (km)	M_L (M_W)*	Seismic moment (dyne cm)*	Number of records
EQ92101	1999/09/20 17:47:15	23°51.15′	120°48.93′	8.0	7.3 (7.6)	3.38×10^{27}	314
EQ92102	1999/09/20 18:03:40	23°47.49′	120°52.58′	3.5	6.6 (6.4)	4.83×10^{25}	184
EQ92106	1999/09/22 00:14:40	23°49.58′	121°02.80′	15.6	6.8 (6.4)	5.03×10^{25}	360
EQ92107	1999/09/25 23:52:49	23°51.56′	121°00.35′	10	6.8 (6.5)	6.01×10^{25}	350

*Harvard CMT Catalog (*www.seismology.harvard.edu*).

and modeled data. Our goal was to show that the empirical data do not contradict the existing source scaling models. The modeled coefficients β_M for magnitude ranges $5.0 < M_L < 7.0$ reveal approximately the same dependence on frequency. Therefore, for the case of empirical data, it is reasonable to use the averaged, for every frequency, values (Figure 1b, dashed line) for estimation of spectral amplitudes for the larger magnitudes ($6.5 < M_L < 7.0$ and $7.0 < M_L < 7.5$, Figure 1a, dashed lines).

The Chi-Chi Earthquake Data

More than 10,000 digital 3-component, strong-motion accelerograms from events of $M_L > 4$ had been recorded in the first 4 weeks after the Chi-Chi earthquake mainshock (Shin *et al.*, 2000). When the research was being carried out, the data from four events (namely, the mainshock and three aftershocks) were processed and compiled in a form suitable for computer (Cheng *et al.*, 2000). The parameters of the events are listed in Table 1. Figure 2 shows epicenters of the earthquakes and locations of free-field, 3-component, accelerograph stations for the recordings used in this study. Figure 3 shows examples of ground-motion acceleration records obtained during the Chi-Chi earthquake mainshock. The spectra of the time histories are shown in Figure 3. Note that most of the stations to the west and south of the epicenter (CHY, KAU, and TCU arrays) are located in a deep alluvium plain area (the Western Coastal Plain, WCP). The long-period waveforms that include significant surface waves, (e.g., station CHY044, Fig. 3) appear to be the common ground motion characteristic in the area (Furumura *et al.*, 2000; Huang and Chen, 2000).

Faulting during the earthquake was interpreted as reverse, left-lateral faulting on a low-angle north–south trending plane. In our study we used one of the source models developed on the basis of teleseismic body waves and strong-motion records (e.g., Furumura *et al.*, 2000; Iwata *et al.*, 2000; Lee and Ma, 2000; Yagi and Kikuchi, 2000); namely, strike 3°; dipping angle 30° to the East; length of the source, 85 km and width, 40 km. These models interpret faulting during the earthquake as faulting along the Chelungpu fault (Fig. 2a). The surface faulting along the Chelungpu fault produced by the earthquake extends north–south about 80–90 km, and has a maximum horizontal slip of about 10 m and a maximum scarp height about 8 m (Lee *et al.*, 2000). The long-period ground velocity pulses are evident at nearly all stations located within 5 km of the Chelungpu fault line. Two stations (TCU52 and TCU68; see Fig. 3) located at a hanging wall at the northern part of the Chelungpu fault exhibit simple one-sided ground movement for a greater than 6-second duration (Huang and Chen, 2000). Our empirical spectral model was developed for average-soil conditions and it does not include such extreme effects as a surface motion near the ruptured fault. Therefore, we did not use records obtained in the vicinity of Chelungpu fault, for comparing empirical and modeled spectra.

When calculating the modeled spectra by equation (1), we used the shortest distance R_{SP} between the source plane (surface of fault slippage) and the station. Figure 4b shows the distribution of PGA values versus R_{SP} for the source-plane model used. It is seen that the ground-motion values tend to saturate at distances less than 10–15 km. The effect can be also seen for the response spectra amplitudes (Fig. 4c, frequency 1 Hz chosen as an example). Actually, the distance of saturation depends on magnitude, and the effect is considered in almost all attenuation models that use different definitions of source-to-site distance. On the other hand, it is natural to suppose that, in the case of a large fault with nonuniform slip distribution, the ground-motion parameters in intermediate- and high-frequency range are mostly determined by distance R_{SH} to the nearest area of high-energy release (see, among others, Gusev, 1983; Arefiev, 1985; Koyama and Zheng, 1985; Aki, 1987; Chernov, 1989). Figure 4d shows the distribution of PGA values versus R_{SH}, where R_{SH} was determined using one of the models for slip distribution along the Chi-Chi earthquake source proposed by Irikura *et al.* (2000). Three asperities or areas of large slip that were selected on the fault plane are shown as shadow zones in Figure 4a, and the R_{SH} values were determined as distance to the center of the nearest asperity. In this case, the minimum R_{SH} values are about 10 km—the above mentioned distance of saturation. Thus, the phenomenon of ground-motion values saturation may be also explained by possible errors in source-to-site distance estimation near the earthquake source (Chernov, 1984, 1989). Note that stations TCU052 and TCU068 are located at a hanging

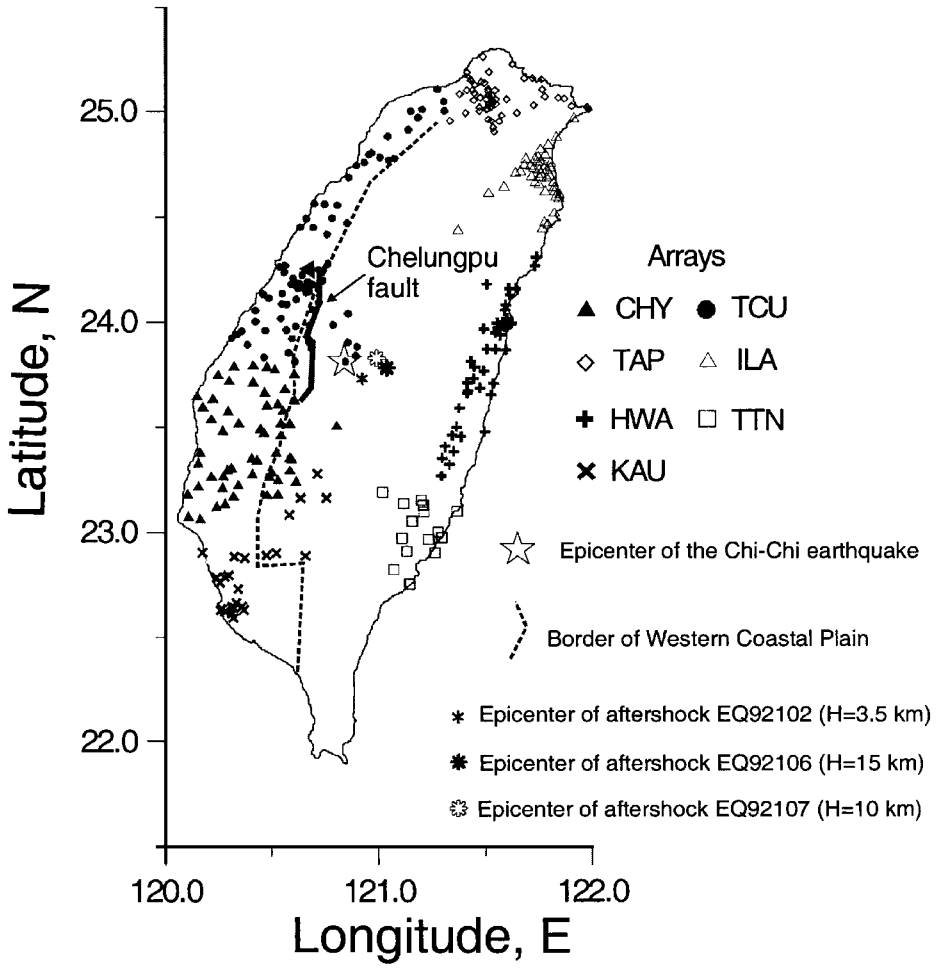

Figure 2. Epicenters of earthquakes (the mainshock and three aftershocks), recordings of which were used in this study, and location of the free-field digital accelerograph stations (TSMIP network).

wall near the Chelungpu fault, and the record obtained at station TCU065 exhibits effects of liquefaction (Wen and Yeh, 2001). At present, it seems to be impossible to evaluate, even if roughly, the peculiarities of slip distribution for future earthquakes. Our goals include evaluating the applicability of the developed spectral model to the case of a large future earthquake, and we assumed that we have information only on the magnitude and general source parameters, (namely, dimensions, strike, and slip angles). Therefore, we used in the study the shortest distance R_{SP} (hereafter referred to simply as *distance*) between the source plane or surface of fault slippage and the station.

The sources of the aftershocks were also modeled as planes (length, 50 km; width, 30 km) with dipping angle (30° to the East) and strike angle (3°) similar to the mainshock. The centers of the source planes coincide with the reported hypocenters. The fault solutions for aftershocks EQ92106 and EQ92107 showed approximately the same faulting as that in the case of the mainshock (reverse faulting), and aftershock EQ92102 is a strike-slip event (Harvard CMT Catalog, *www.seismology.harvard.edu*).

Comparison of Empirical and Modeled Data

Fourier Amplitude Spectra

The Chi-Chi Earthquake Aftershocks. Let us begin the comparison between observed and modeled spectra from the aftershock data. Magnitudes of the aftershocks considered (see Table 1) lay within the first interval of magnitudes ($6.5 < M_L < 7.0$), for which the reference spectrum was evaluated using the coefficients β_M. On the one hand, the comparison between the observed and modeled Fourier amplitude spectra of ground acceleration may be performed by dividing the observed spectra into groups by means of distance (25–35 km, 45–55 km, etc.) and calculating the modeled spectra for centers of the intervals. On the other hand, it is possible to recalculate the observed spectra to a certain distance using equation (1) and to compare the data with the modeled spectrum. In the second case, all observed records are used, although the azimuth- and distance-dependent peculiarities are averaged. We used both variants in our study.

In the case of aftershock EQ92106 (M_L 6.8, hypocentral

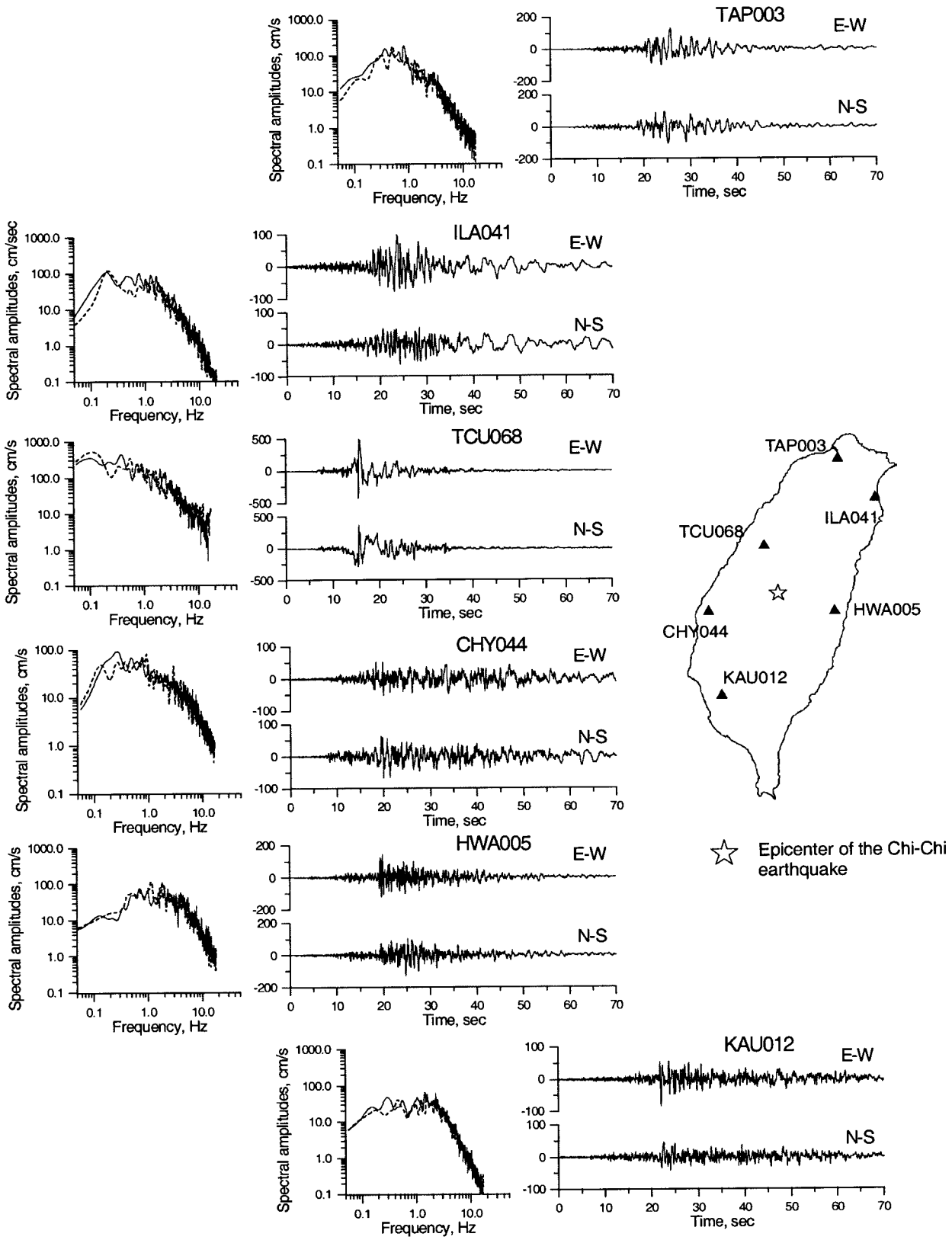

Figure 3. Examples of the data from the Chi-Chi earthquake mainshock: acceleration time histories (amplitudes in cm/sec^2), and spectra of accelerograms (solid lines: E–W component; dashed lines: N–S components).

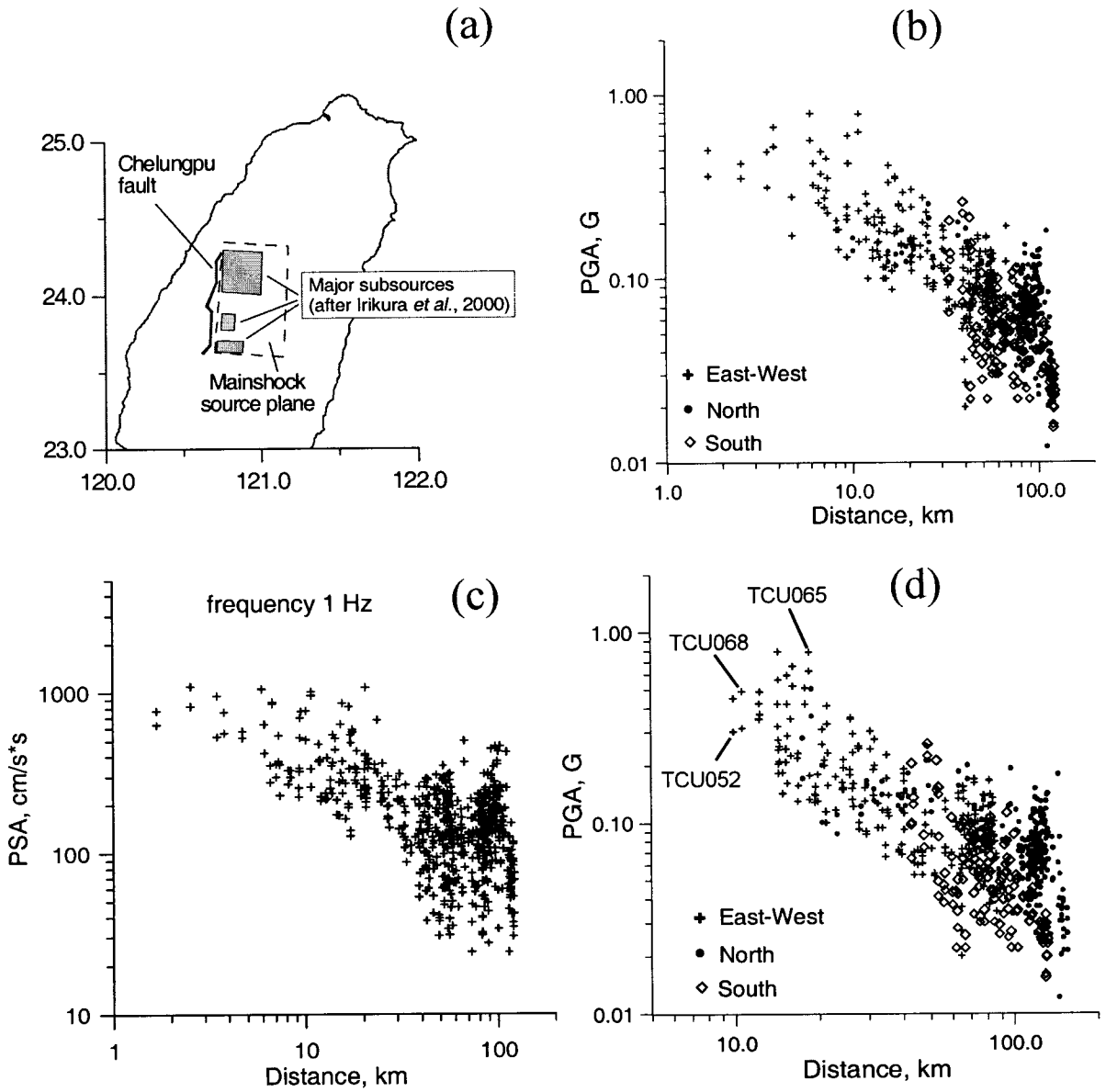

Figure 4. The Chi-Chi mainshock data. (a) Location of the Chelungpu fault, projection of the source plane on the Earth surface and location of major subsources (Irikura *et al.*, 2000). (b) Distribution of the peak ground acceleration (PGA) values versus shortest distance between station and the source plane. (c) Distribution of the response spectra amplitudes versus shortest distance between station and the source plane. (d) Distribution of the PGA values versus distance between station and center of the nearest subsource.

depth 15 km), the attenuation of seismic waves was considered to be $Q = 125\, f^{0.8}$. Comparison of the modeled and observed spectra for the aftershock shows a very good agreement (Fig. 5a), both by shape and amplitude. Figures 5b and 5c show a typical relation between the spectra observed in the eastern (arrays HWA, ILA, and TTN) and the western parts of the island (the Western Coastal Plain, arrays CHY, TCU and KAU). The stations located in deep alluvium plain area (the Western Coastal Plain) are characterized by higher spectral amplitudes at frequencies less than 1 Hz compared to those for eastern direction. The ratio between the western and eastern spectra (Fig. 5c) increase with decrease of frequency up to 2.8–2.5 at frequencies about 0.1–0.2. It is natural to suppose that the difference reflects the influence of deep deposits on ground motion.

Preliminary analysis of the data from aftershock EQ10297 (M_L 6.8, hypocentral depth 10 km) showed that the high-frequency amplitudes of the observed spectra are characterized by lower values than those predicted by the model with attenuation $Q = 125\, f^{0.8}$ (Fig. 6a). Therefore,

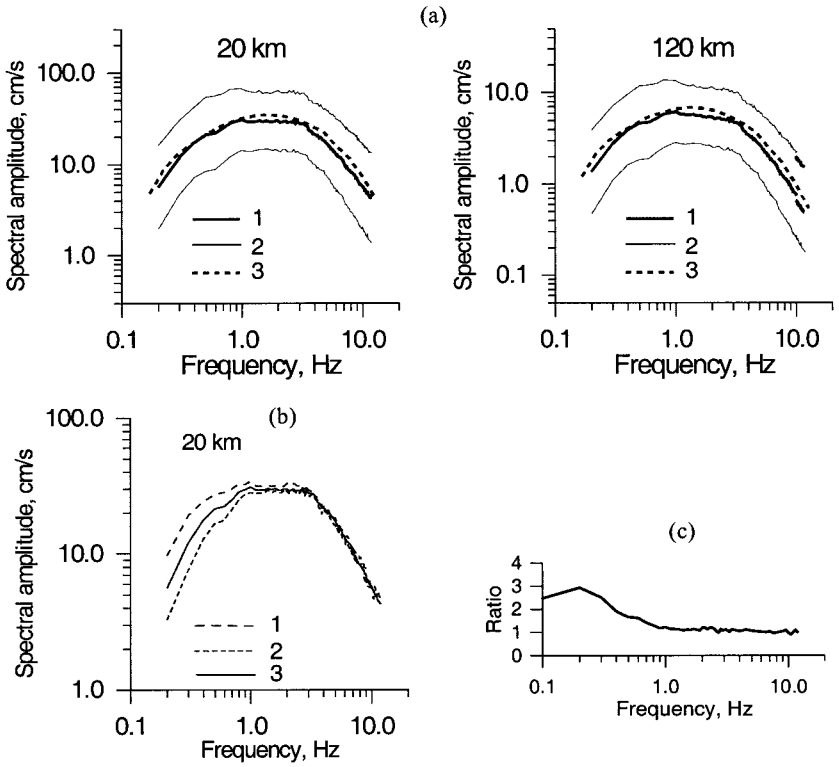

Figure 5. Aftershock EQ92106 (M_L = 6.8, H = 15 km). (a) Comparison between observed Fourier amplitude spectra of ground acceleration (1: the mean values; 2: mean ± 1 st. deviation limits), and simulated, using average-soil model (line 3), spectra ($6.5 < M_L < 7.0$). The observed spectra were recalculated to distances 20 km and 120 km using equation (1) and $Q(f) = 125\, f^{0.8}$. (b) Comparison of observed spectra recalculated to distance 20 km (1: data from the Western Coastal Plain; 2: data from the eastern part of the island; 3: all data). (c) Ratio between averaged observed spectra from western and eastern parts of the island.

we estimated a new Q-model, using the approach applied in our previous study (Sokolov *et al.*, 2000). When considering records from a single earthquake, apart from source-dependent variations (peculiarities of the rupture process), the difference between spectral amplitudes at a given frequency is caused by distance-dependent attenuation and site-dependent amplification factors. When partially removing spectral amplitude and shape modification multiplying by $R^b \exp[\pi f R/Q(f)\beta]$ (i.e., recalculating to reference distance), the scatter of spectral amplitudes, ideally, is determined only by source- and site-dependent factors. Let us suppose that site amplification for the same ground condition does not depend on shaking intensity. Therefore, the proper attenuation model should provide minimum variance of the spectral amplitudes $|A|$ for all considered frequencies at reference distance. Thus, it is necessary to analyze values $D_A = (\Sigma D_f)/N_f$ obtained for different attenuation models. Here D_f is the variance of $\log_{10}|A|$ values at frequency f; D_A is the arithmetic average of the D_f values; N is the number of frequencies used. The requirement of minimum arithmetic average D_A is not sufficient, however. Actually, the D_A value does not consider variations of the D_f values at different frequencies, and the optimal attenuation model requires for uniform scatter of $\log_{10}|A|$ over the entire frequency range. To consider this requirement, it is necessary also to analyze values of the ratio $D_{GA} = D_G/D_A$, where $D_G = (D_1 \times D_2 \times \ldots \times D_N)^{1/N}$ is the geometric average of the values D_f at frequency f_i. The ratio D_{GA} approaches unity under a condition of approximately equal values of variance at considered frequencies.

For the case of aftershock EQ92107, the distributions of D_A and D_{GA} values were analyzed for various attenuation models $Q(f) = Q_0 * f^n$, and it has been found that the optimal models are characterized by values of Q_0 = 70–90 and n = 0.8–0.9. The standard deviation of reference-distance spectral amplitudes does not exceed 0.25 log unit. When using attenuation $Q = 80\, f^{0.8}$, the modeled spectra in the case of aftershock EQ92107 reveal a better agreement with the observed spectra (Fig. 6b). Note that in a previous study of $Q(f)$ relations for the Taiwan region (Wang, 1993) the relation $Q(f) = 98\, f^{1.0}$ was proposed for earthquakes with hypocentral depth less than 11 km.

Figure 6c shows a relation between the spectra observed during the event in the eastern part (arrays HWA, ILA, and TTN) and the western part of the island (the Western Coastal Plain, arrays CHY, TCU, and KAU). The ratios between the western and eastern spectra that were calculated for the considered aftershocks (EQ92107 and EQ92107) are compared in Figure 6d. The curves exhibit almost the same influence of the Western Coastal Plain on ground motion during the events.

In the case of aftershock EQ92107, the empirical spectra, in general, reveal higher amplitudes than the modeled spectra at frequencies 0.4–0.5 to 2–3 Hz (Fig. 6b). The phenomenon could be seen both for the eastern and western spectra (Fig. 6e). Therefore, it is possible to suppose that the difference reflect the intrinsic peculiarity of the EQ92107 event. Figure 6f compares the ratios between the averaged empirical spectra (all stations) and corresponding modeled spectra for aftershocks EQ92106 and EQ92107. The data for

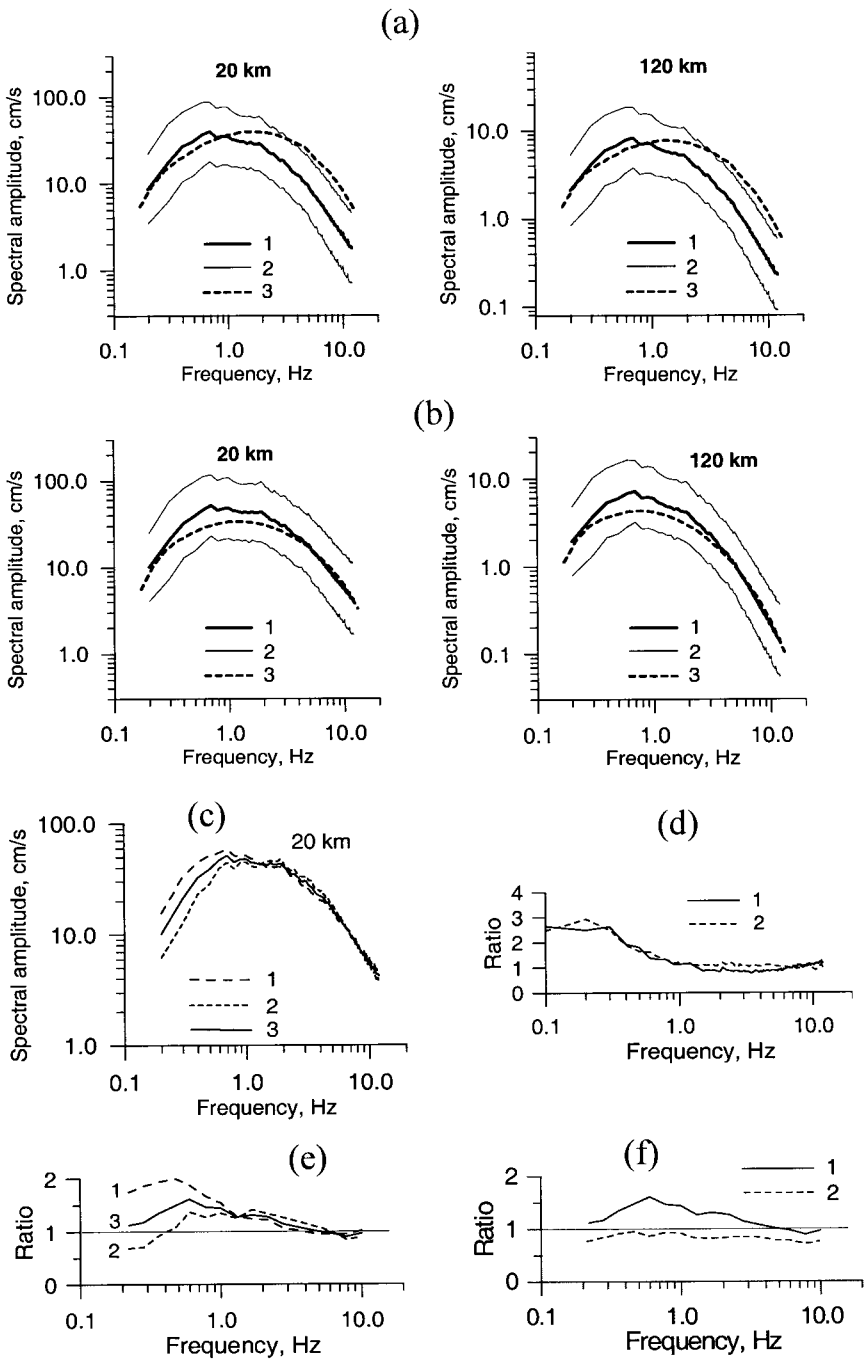

Figure 6. Aftershock EQ92107 (M_L = 6.8, H = 10 km). (a, b) Comparison between observed Fourier amplitude spectra of ground acceleration (1: mean values; 2: mean ± 1 st. deviation limits), and simulated, using average-soil model (line 3), spectra ($6.5 < M_L < 7.0$). The observed spectra were recalculated to distances 20 km and 120 km using two Q-models, namely: $Q(f) = 125\,f^{0.8}$ in (a) and $Q(f) = 80\,f^{0.8}$ in (b). (c) Comparison of observed spectra recalculated to distance 20 km (1: data from the Western Coastal Plain; 2: data from the eastern part of the island; 3: all data). (d) Comparison of ratios between spectra from western and eastern parts of the island for aftershocks EQ92107 (curve 1) and EQ92106 (curve 2). (e) Comparison of ratios between the observed and modeled spectra for aftershocks EQ92107 (1: western spectra; 2: eastern spectra; 3: all observed data). (f) Comparison of ratios between the observed and modeled spectra for aftershock EQ92107 (line 1, all observed data) and EQ92106 (line 2; see also Fig. 5c).

aftershock EQ92107 show the mentioned amplification, and the ratios for aftershock EQ92106 exhibit amplitudes that are close to unity for the whole range of frequencies considered.

The aftershock 92102 (M_L 6.6, depth 3.5 km) occurred 16 minutes later than the mainshock and 6 minutes later than the other large (M_L 6.1) aftershock. Therefore, there were several problems with identification and timing of the numerous records obtained during the first few hours after the mainshock (Cheng *et al.*, 2000). Moreover, due to technical reasons several records of the aftershock are characterized by short duration (less than 30 seconds) of ground motion. The records do not include the most intensive part of ground motion. Figure 7a shows the acceleration records obtained near the source (source–site distance less than 15 km) and in the farfield zone (distance 50 km) and their spectra. It is seen that the ground motion, even in the near-field zone, is characterized by presence of intensive long-period components that appear from the very beginning of the excitation. Figure 7b shows a comparison of the observed and modeled spectra for the aftershock. The modeled spectra were obtained using the models for two magnitude intervals ($6.0 < M_L < 6.5$ and $6.5 < M_L < 7.0$) and attenuation relation $Q = 80 f^{0.8}$. The observed spectra exhibit larger low-frequency amplitudes and lower high-frequency amplitudes than for the models, and the discrepancy is very high.

Figure 7c shows a typical relation between the spectra observed in the eastern part and the western part of the island during the aftershock. The stations located in the deep alluvium plain area (the Western Coastal Plain) are characterized by higher spectral amplitudes at frequencies less than 2–3 Hz than those for the eastern direction. The comparison of the averaged ratios between western and eastern spectra for the considered aftershocks is shown in Figure 7d. All the events reveal an increase of spectral amplitudes with decrease of frequency for deep alluvium plain. The shallow event EQ92102 is also characterized by prominent amplification of spectral amplitudes at frequency range of 0.3–0.8 Hz. In this case, it is not possible to compare the observed spectra with the model; however, bearing in mind the spectral amplification for event EQ92107 within the corresponding frequency range (Fig. 6e), we can suppose that the phenomenon of increased spectral amplitudes relates to the depth of the earthquakes in the central part of Taiwan island (the so-called shallow-earthquake effect). Of course, the supposition is quite preliminary, and it should be verified on the basis of other shallow earthquakes.

It has been already noted that aftershock EQ92102, in addition to its very shallow hypocentral depth, is characterized by strike-slip faulting. Therefore, we do not use the data from this event for further analysis. In contrast to other studied events, the parameters of the earthquake do not satisfy the general characteristics of the data used for development of the empirical spectral model. The model was obtained on the basis of earthquakes of mostly reverse faulting and hypocentral depth more than 5 km.

The Chi-Chi Earthquake Mainshock. Before comparison of the data from the mainshock and modeled spectra, we should make the following notes. First, when using records obtained in the epicentral zone (distances less than 10–15 km), we did not include the records obtained at stations located along the Chelungpu fault. We also did not include in our analyses the following data: (a) several records of the TCU array obtained in a liquefied area (Wen and Yeh, 2001); (b) records obtained in the central part of the alluvium-filled Langyang basin (ILA array), which include significant surface waves (Liu and Wen, 2000; see station ILA041 in Fig. 3, as an example); and (c) records obtained in the central part of the Taipei basin (TAP array), which show a strong basin response on the earthquake (Tsai and Huang, 2000; Tsai *et al.*, 2000; Fletcher, 2001). Second, we consider the accelerograms recorded in the Western Coastal Plain (see Fig. 2) as a separate dataset due to the presence of surface waves. Third, the models of rupture process show unilateral northward propagation (Furumura *et al.*, 2000; Lee and Ma, 2000; Yagi and Kikuchi, 2000; see also *http://wwweic.eri.u-tokyo.ac.jp/yuji/taiwan/taiwan.html*). Therefore, we divided the data both by means of distance and direction from the source. In this case we used a distance increment of 10 km and the intervals containing less than five records were not considered. The average-soil spectral model for magnitude interval $7.0 < M_L < 7.5$ (Fig. 1a) was used and the modeled spectra were calculated for centers of corresponding distance intervals using Q-model $Q(f) = 80 f^{0.8}$.

Figure 8 shows the comparison between simulated and observed Fourier amplitude spectra of ground acceleration for the epicentral area (distance less than 15 km) and eastern and western directions. The data set for the epicentral area contains spectra from six stations (TCU71, TCU72, TCU76, TCU79, TCU84, and TCU89) located to the east from the Chelungpu fault (see Fig. 2). For the eastern and western stations, all spectra were recalculated to distance 40 km. The modeled spectra calculated for corresponding distances show, in general, a good agreement with the mean amplitudes of the observed spectra at frequencies 0.3–12 Hz both for epicentral area and eastern direction (HWA array; see also Fig. 2). The data from epicentral area, however, exhibit lower spectral amplitudes than the modeled spectrum for frequencies 0.3–1.0 Hz. On the one hand, the difference may relate to so-called finite-fault effect (i.e., the peculiarities of strong ground motion near the extended fault); two-corner-frequency spectral models were developed to satisfy the peculiarities (e.g., Atkinson, 1993; Atkinson and Silva, 2000). On the other hand, most of the near-field stations used belong to soil class D (Lee *et al.*, 2001). In general, the type of site condition in the Taiwan region is characterized by amplification at frequencies greater than 1 Hz. Thus, the difference between recorded and modeled spectra may also relate to difference between class D and broadband average-soil amplifications.

In the case of eastern data, the empirical spectra, in general, reveal the higher amplitudes than the modeled spectra

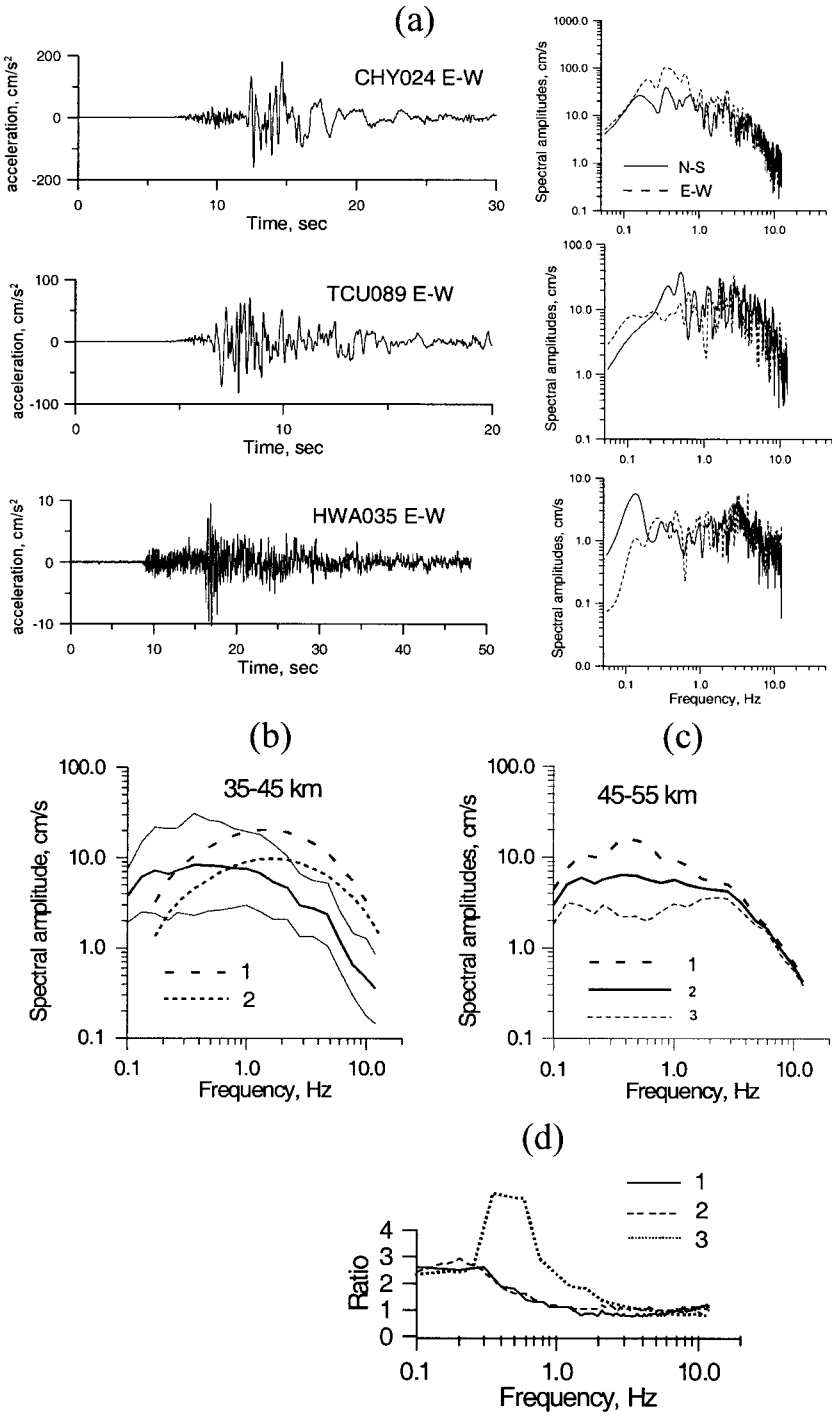

Figure 7. Aftershock EQ92102 (M_L = 6.6, H = 3.5 km). (a) Acceleration records and spectra obtained at distances less than 15 km (CHY024 and TCU089) and about 50 km (HWA035). (b) Comparison between observed Fourier amplitude spectra of ground acceleration (solid lines show the mean values, thick line, and mean ± 1 st. deviation limits, thin line), and simulated, using average-soil model (dashed lines), spectra (line 1 represents magnitude interval $6.5 < M_L < 7.0$; line 2, $6.0 < M_L < 6.5$). (c) Comparison of averaged spectra, distance interval 45–55 km (1: data from the Western Coastal Plain; 2: data from the eastern part of the island; 3: all data). (d) Comparison of average ratios between spectra from western and eastern parts of the island for aftershocks EQ92107 (curve 1), EQ92106 (curve 2), and EQ92102 (curve 3).

at frequencies from 0.7–0.8 Hz to 2–3 Hz. The same phenomenon could be seen for the southern stations (Fig. 9a) and for the case of the shallow aftershock EQ92107 (Fig. 6b).

The spectra from the western direction (stations of the CHY and TCU arrays located in the Western Coastal Plain) show a good agreement with modeled spectra at frequencies greater than 0.7–0.8 Hz but exhibit sufficiently larger amplitudes at frequencies less than 0.6–0.7 Hz. Obviously, the difference is caused by surface waves generated by the mainshock in this area (Furumura *et al.*, 2000; Huang and Chen, 2000). The influence of surface waves on ground-motion spectra can be seen also in the southern (Fig. 9a) and northern (Fig. 10a) subsets of the data from Western Coastal Plain area (arrays CHY, KAU, and TCU).

The average spectral amplitudes of ground acceleration recorded to the south from the source outside the Western Coastal Plain (Fig. 9a) show higher amplitudes at frequen-

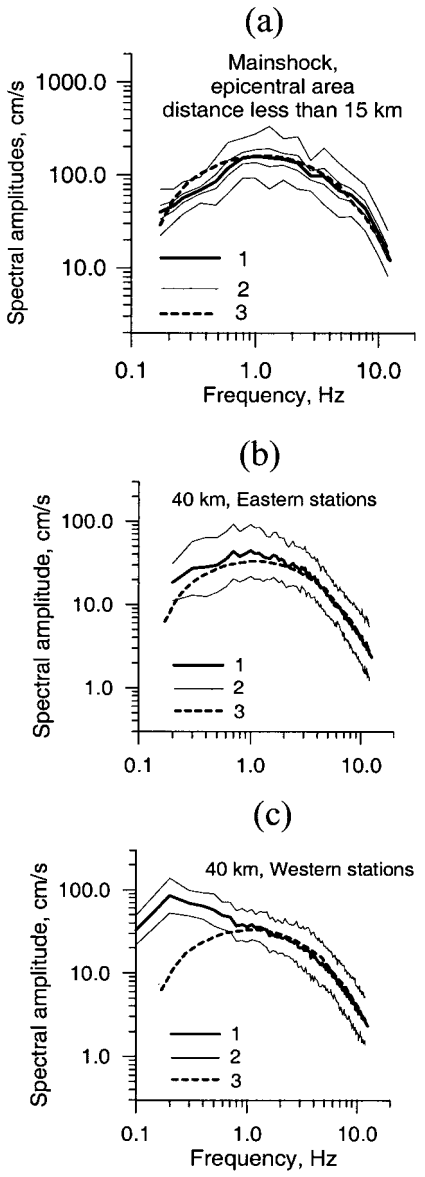

Figure 8. The Chi-Chi earthquake mainshock, comparison between observed Fourier amplitude spectra of ground acceleration and simulated, using average-soil model (dashed lines), spectra (magnitude interval $7.0 < M_L < 7.5$). (a) Epicentral area (1: mean values of the observed spectra; 2: mean $\pm$ 1 st. deviation of the mean, and mean $\pm$ 1 st. deviation limits; 3: modeled spectrum). (b,c) Data from the eastern part of the island and from the Western Coastal Plain recalculated to distance 40 km (1: mean values of the observed spectra; 2: mean $\pm$ 1 st. deviation limits; 3: modeled spectrum).

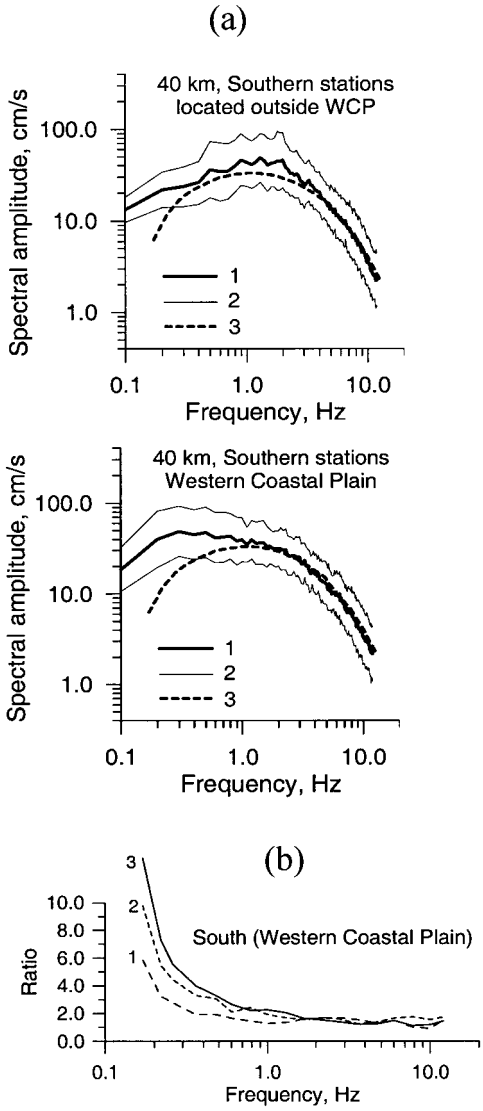

Figure 9. The Chi-Chi earthquake mainshock, southern data. (a) Comparison between Fourier amplitude spectra of ground acceleration observed in the areas outside and within the Western Coastal Plain (WCP), and simulated, using average-soil model, spectra. Curves are as in Fig. 8. (b) Comparison of ratios between averaged spectra from the Western Coastal Plain and modeled spectra (1: distance interval 45–55 km; 2: 55–65 km; 3: 75–85 km).

cies less than 0.2–0.3 Hz than the modeled spectra but reveal a good agreement with the model for frequencies greater than 0.3 Hz. The spectra of accelerograms recorded in the Western Coastal Plain exhibit higher amplitudes, compared with the modeled ones, for frequencies less than 2–3 Hz, and the difference increases with distance (Fig. 9b). The same relationship between observed and modeled spectra can be seen for the northern spectra (Fig. 10a,b); however, in this case the difference becomes significant (ratios between observed and empirical amplitudes more than 1.3–1.5) for frequencies less than 2–3 Hz also for areas located outside the Western Coastal Plain (namely, the northern and northeastern part of the island, TAP and ILA arrays). Thus, it is possible to conclude that the ground motions outside the Western Coastal Plain also contain surface waves at distances more than 40–50 km to the south and north of the mainshock source. The influence of surface waves for the Western

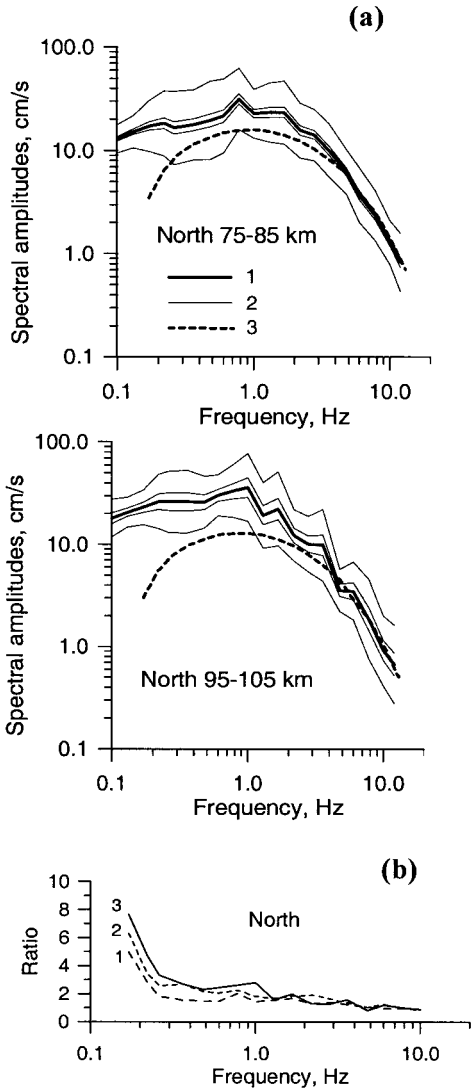

Figure 10. The Chi-Chi earthquake mainshock, northern data. (a) Comparison between Fourier amplitude spectra of ground acceleration observed in the areas outside the Western Coastal Plain (WCP), and simulated, using average-soil model, spectra. Curves are as in Fig. 8. (b) Comparison of ratios between averaged northern spectra and modeled spectra (1: distance interval 75–85 km; 2: 85–95 km; 3: 95–105 km).

Coastal Plain (WCP) is important for frequencies less than 1–2 Hz and it becomes predominant for frequencies less than 0.3–0.2 Hz. The frequencies 0.3–0.2 Hz can also be considered as a high-border frequency of the surface waves for the territories located outside WCP to the south and north from the earthquake source.

Figures 11a and 11b compare observed spectra from the WCP area for the same distance interval (45–55 km) and different directions from the source (west, north, and south). In general, the northern spectra are characterized by the highest amplitudes for frequencies less than 1–2 Hz. On the one hand, this phenomenon, as well as the relatively higher amplitudes of the northern spectra in this frequency range for distances 75–105 km (Fig. 10), may be explained by the directivity effect due to northward propagation of the rupture. On the other hand, the influence of propagation-path peculiarities may be also considered as a source of the discrepancy. Furumura *et al.* (2000) on the basis of numerical 2D and 3D simulation concluded that strong diving *S*-waves, produced by the large shallow asperity of the Chi-Chi earth quake and the large velocity gradient in the crust rigid bedrock, enhance the ground motion to the north from the source at epicentral distances of about 80 and 120 km at frequencies less than 1 Hz. At the same time, the western spectra exhibit higher low-frequency ($<$0.3 Hz) amplitudes than the southern spectra, showing the stronger influence of surface waves in this direction.

Figure 11c compares average values of observed spectra for the same distance interval and different direction from the source and location of the stations. On the one hand, it is possible to see the influence of surface waves in the low-frequency range: the spectra from WCP area exhibit higher amplitudes than those for the areas outside the WCP at frequencies greater than 0.8–1.0 Hz. On the other hand, the southern WCP spectra are characterized by lower amplitudes in low-frequency range than for the northern spectra, reflecting the effect of directivity of rupture propagation. Comparison of the northern (outside WCP) and southern (WCP) spectra (distances 75–85 km) shows that the influence of deep-alluvium plain (surface waves and response of deep deposits) is much stronger than the directivity effect for frequencies less than 1 Hz.

Finally, we compared the ratios of spectral amplitudes between the data from western and eastern parts of the island (west–east spectral ratios) evaluated for the mainshock and two aftershocks EQ92106 and EQ92107, for distances less than 50–55 km (Fig. 12). In this case, the mainshock data do not include the above-mentioned effects of rupture propagation and shallow crust structure. Therefore, the data show peculiarities of response of deep alluvium deposits (the Western Coastal Plain) during relatively large earthquakes of various depths. On the one hand, the increase of amplitudes of the ratios with decrease of frequency reflects the general characteristics of deep deposits response on ground motion. On the other hand, the west–east spectral ratio for the mainshock, showing approximately the same values as in the case of aftershocks for frequencies greater than 0.4 Hz, exhibits very high amplitudes for frequencies less than 0.3 Hz. Most probably, the phenomenon reflects the influence of surface waves in the Western Coastal Plain.

Peak Ground Acceleration. We performed the comparison of peak ground accelerations observed during the considered events of the Chi-Chi earthquake sequence and modeled PGAs on the basis of average-soil spectral models. The modeled PGA values were calculated using stochastic simulation technique (Boore, 1983). One of the most important param-

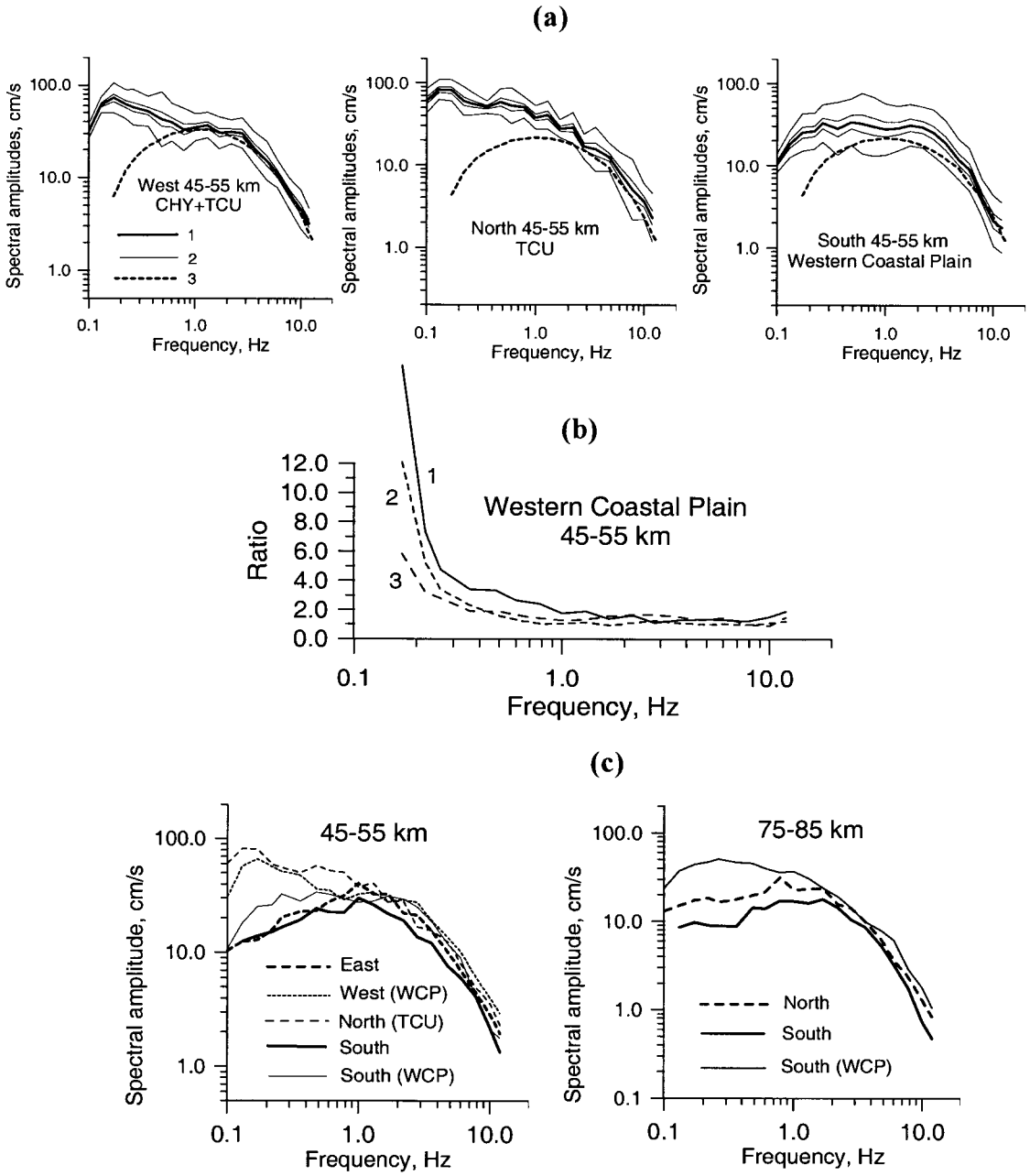

Figure 11. The Chi-Chi earthquake mainshock, data for the similar intervals of distance. (a) Comparison between Fourier amplitude spectra of ground acceleration observed in different directions from the source plane and simulated, using average-soil model, spectra. Curves are as in Fig. 8. (b) Comparison of ratios between averaged observed spectra from Western Coastal Plain and modeled spectra (1: northern direction; 2: western direction; 3: southern direction). (c) Comparison of averaged empirical spectra for various directions and distances from the source.

eters of the stochastic predictions is the duration model, because it is assumed that most (90%) of the spectral energy is spread over a duration $\tau_{0.9}$ (the so-called significant duration) of the accelerogram. It has been found in our previous study (Sokolov *et al.*, 1999, 2000) that usage of the regional relationship between ground motion duration ($\tau_{0.9}$) and magnitude proposed by Wen and Yeh (1991) in the following form,

$$\tau_{0.9} = 0.43\exp(0.504\ M_L) \pm 2.749, \qquad (4)$$

gives a good fit to empirical data. A mean value of 17 sec should be used for earthquake of magnitude M_L 7.3 according to the relationship. We made an attempt to evaluate the duration–distance relationships on the basis of the registered accelerograms. The duration is defined as the interval between the times at which 5% and 95% of the Arias intensity

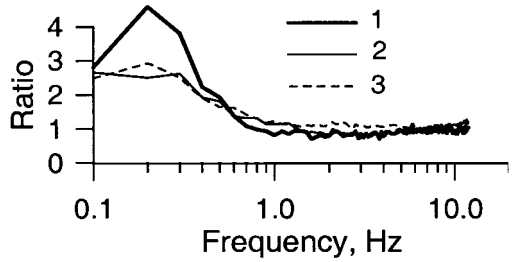

Figure 12. Comparison of ratios between observed spectra from western and eastern part of the island (1: the Chi-Chi earthquake mainshock; 2: aftershock EQ92107; 3: aftershock EQ92106).

integral is attained (Trifunac and Brady, 1975). We use the average-soil spectral model in our comparison; therefore, it is necessary to estimate the durations excluding such extreme effects as propagation of long-period surface waves along the alluvial basins (the Western Coastal Plain and the Lanyang basin; Fig. 13a). The high-pass filtering procedure was applied to every accelerogram, and we calculated the duration of ground motion in the frequency range above 0.4 Hz. In this case the influence of the location-dependent long-period waves, which had been observed along the Chelungpu fault, was also eliminated.

The distribution of the significant duration versus distance for the mainshock is shown in Figure 13b. In general, duration reveals no dependence on distance, at least for the northern and east–west directions from the source plane. On the other hand, as shown in Figure 13c, the duration values for southern ground motions increase with distance and the dependence may be described as $\tau_{0.9} = 5.2\ R^{0.44}$. Table 2 lists the statistical parameters of ground-motion duration determined for the entire data set, and for the stations at different directions from the source. The influence of rupture directivity could be clearly seen: the effective duration of ground-motion acceleration toward the south from the source is, in general, 1.4–1.5 times higher than that toward the north. At the same time, the duration along the east–west direction may be considered as the average one, and the mean value of 22 sec is close to that predicted by the Wen and Yeh's relationship (17 sec $\pm$ 2.75 sec).

It has been shown above that the average-soil spectral model shows a good agreement with the observed spectra for frequencies greater than 0.4 Hz where the influence of surface waves is not dominant. Therefore, for comparison we used the PGA values determined from the filtered accelerograms. Actually, the difference between original and filtered PGAs does not exceed 25%. Figure 14a shows the comparison between empirical PGA (horizontal components, filtered accelerograms) and those calculated using the empirical average-soil spectra. We do not include in the comparison the data from two stations (TCU068 and TCU052) located at the hanging wall near the Chelungpu fault and from station TCU065 located in a liquefied area. A set of 40 synthetic acceleration time functions was generated for effective duration of 20 sec, and the resulting PGA is estimated as an average value. In this case we consider a hypothetical situation: we have got information about the future earthquake (magnitude and source parameters) and, based on existing empirical models (average-soil spectra and

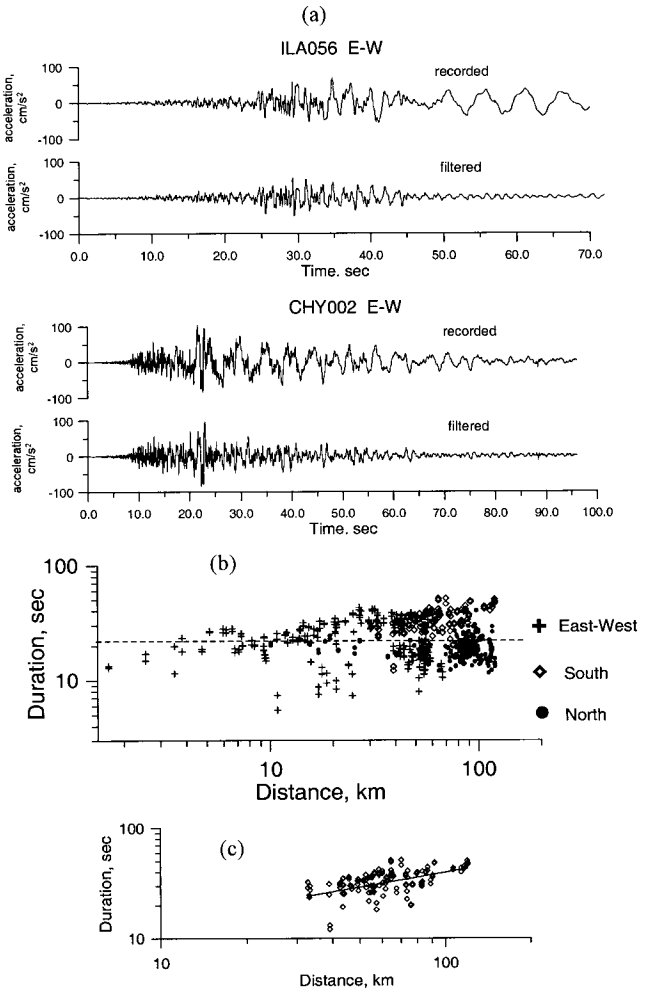

Figure 13. Evaluation of significant duration of ground acceleration during the Chi-Chi earthquake. (a) Examples of recorded and filtered (high-pass above 0.4 Hz) accelerograms. (b) Distribution of significant duration versus distance; dashed line shows average value, 22 sec (Table 2). (c) Values of significant duration for the southern direction from the source; the line shows the duration–distance relationship ($\tau_{0.9} = 5.2\ R^{0.44}$).

Table 2
Results of the Effective Duration Estimation for Mainshock of the Chi-Chi Earthquake

Statistical parameters of the effective duration (τ)	All Data	North	South	East–West
Average value, seconds	22.2	18.4	32.77	22.15
Standard deviation of $\log_{10} \tau$	0.16	0.09	0.11	0.16

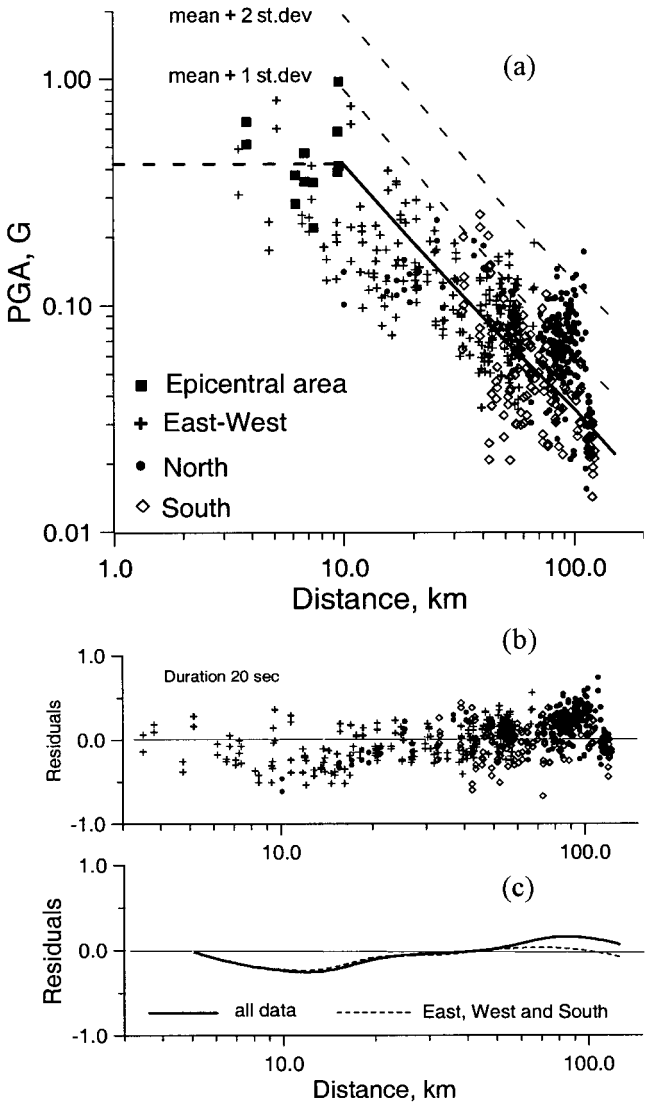

Figure 14. Results of application of the average-soil spectral models for evaluation of peak acceleration for the Chi-Chi earthquake mainshock. (a) Comparison between PGA values (horizontal components) observed during the mainshock (the data from different directions from the source are shown by different symbols) and peak ground accelerations (lines) predicted using the average-soil spectral model ($7.0 < M_L < 7.5$, $Q(f) = 80f^{0.8}$, duration 20 sec). The solid line shows the PGA calculated using the mean values of spectral amplitudes; the dashed lines show mean + 1 and mean + 2 standard deviation. (b) Residuals for peak ground acceleration as a function of distance. The residuals are defined as the ratio between the observed data and PGA values predicted using average-soil spectra. (c) Model bias (average residual) for the entire data set (solid line) and for the subset that does not contain the northern data (dashed line).

effective duration), the distribution of PGA values is evaluated for a scenario earthquake. When calculating theoretical PGAs, the minimum site–rupture distance or distance of saturation to be used in equation (1) was accepted as $R_{MIN} = 10$ km (see also the earlier section, The Chi-Chi Earthquake Data).

The average-soil model combined with an effective duration of 20 sec, in general, provides a satisfactory prediction for the case of the mainshock (Fig. 14b,c); however, the observed peak amplitudes at distances from 6–7 to 15–20 km are lower than the modeled values. The dataset for this distance range contains the records from stations, located to the west from the Chelungpu fault (footwall). As a rule, the footwall stations are characterized by relatively low peak acceleration as compared with that of a hanging-wall location. The hanging-wall near-field data (stations TCU071, TCU072, TCU076, TCU079, TCU084, and TCU089; marked as black squares in Fig. 14a) show a good agreement with the modeled PGA. On the other hand, the modeled amplitudes are lower than the empirical ones for distances more than 60–70 km. The discrepancy may be explained by the above-mentioned general tendency of the northern ground motion to exhibit relatively higher spectral amplitudes due to peculiarities of source rupture and propagation path. When removing the northern data from analysis, the average residuals are almost equal to zero (no bias) for distances more than 20 km. The overall average value of residuals is about 0.033 for the entire data set, and about -0.04 when the northern data were not included. The standard deviation of residuals is about 0.20–0.22 log unit. We also modeled the peak accelerations using the mean average-soil spectra plus 1 and 2 standard deviation values (Fig. 14a, dashed lines). The standard deviation of the average-soil model for magnitudes $6.5 < M_L < 7.5$ has been accepted as average (0.33 log unit) between the values for the empirical reference spectra (see Fig. 1a). It is seen that the mean plus 1 standard deviation spectral model provides an upper limit of peak acceleration for distances less than 30–40 km, and the mean plus 2 standard deviation model also overlaps the effect of the Taipei basin response.

The distribution of significant duration versus distance for aftershock EQ92106 (Fig. 15a) reveals an increase of duration with increasing distance. The dependence may be described as $\tau_{0.9} = 1.29\,R^{0.56}$ or $\log_{10}\tau_{0.9} = (0.11 \pm 0.054) + (0.56 \pm 0.028)\log_{10} R$. Therefore, when applying the average-soil spectral model (magnitude range $6.5 < M_L < 7.0$) for calculation of peak acceleration, the PGA values were determined using the distance-dependent effective duration. Frequency-dependent attenuation of spectral amplitudes was described by $Q(f) = 125\,f^{0.8}$. Figure 15b shows the distribution of the recorded PGA values versus the shortest distance to the surface of fault slippage for the aftershock and comparison with the modeled values. The average value of residuals between the observed data and modeled, using the mean spectra, PGAs (model bias) is about 0.011 and

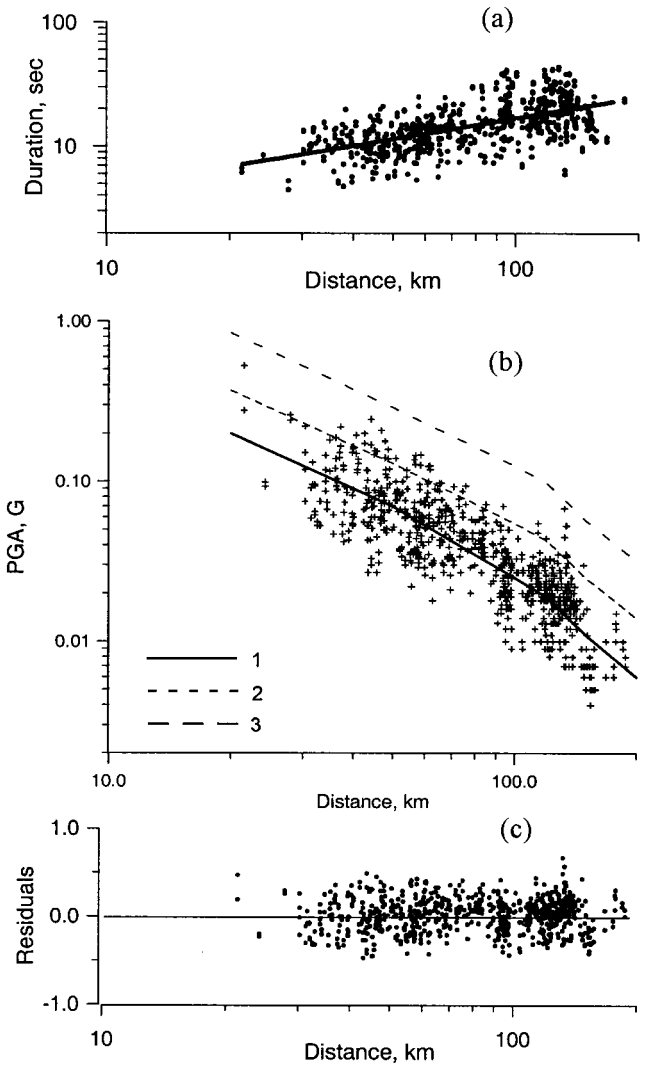

Figure 15. Aftershock EQ92106 (M_L = 6.8, H = 15 km). (a) Distribution of significant duration $\tau_{0.9}$ versus distance; the line shows the duration–distance relationship ($\tau_{0.9}$ = 1.29 $R^{0.56}$). (b) Comparison between observed PGA values (horizontal components) and peak ground accelerations predicted using the average-soil spectral model ($6.5 < M_L < 7.0$, $Q(f)$ = 125 $f^{0.8}$). The solid line (1) shows the PGA calculated using the mean values of spectral amplitudes; the dashed lines show mean + 1 (line 2) and mean + 2 (line 3) standard deviation. (c) Residuals for peak ground acceleration as a function of distance. The average value of residuals (model bias) is about 0.011 and the standard deviation of residuals is 0.19 log unit.

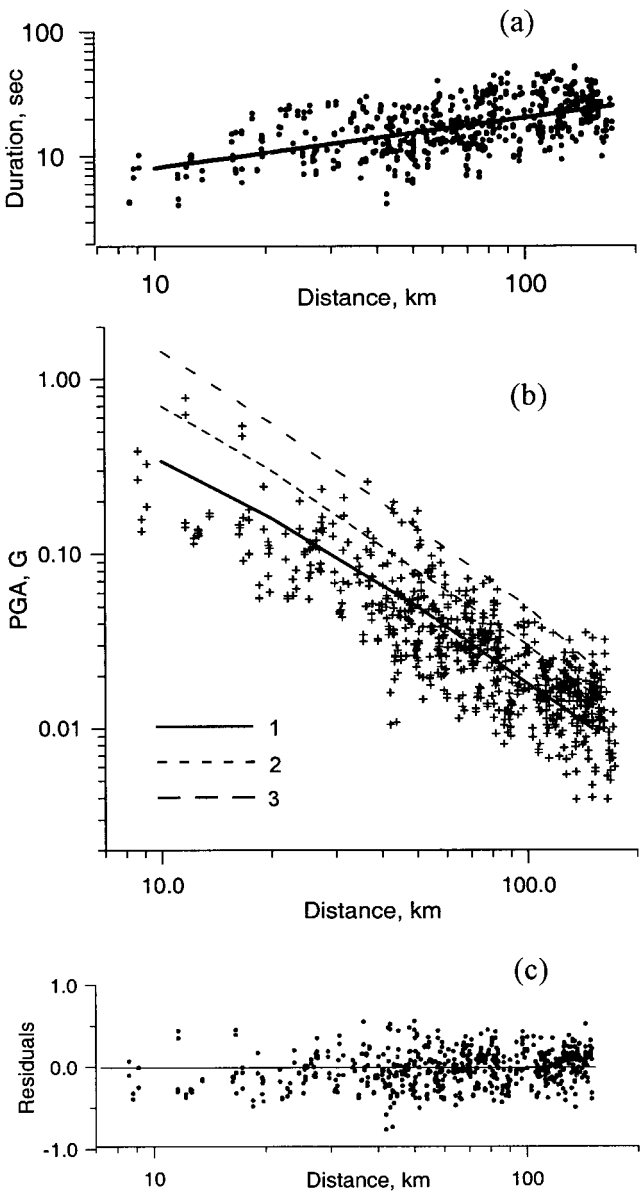

Figure 16. Aftershock EQ92107 (M_L = 6.8, H = 10 km). (a) Distribution of significant duration $\tau_{0.9}$ versus distance; the line shows the duration–distance relationship ($\tau_{0.9}$ = 3.64 $R^{0.37}$). (b) Comparison between observed PGA values (horizontal components) and peak ground accelerations predicted using the average-soil spectral model ($6.5 < M_L < 7.0$, $Q(f)$ = 80 $f^{0.8}$). The solid line (1) shows the PGA calculated using the mean values of spectral amplitudes; the dashed lines show mean + 1 (line 2) and mean + 2 (line 3) standard deviation. (c) Residuals for peak ground acceleration as a function of distance. The average value of residuals (model bias) is about −0.03 and the standard deviation of residuals is 0.21 log unit.

standard deviation of residuals is about 0.19 log unit (Fig. 15c).

Figure 16a shows the distribution of significant duration versus distance for the aftershock EQ92107. In this case the duration $\tau_{0.9}$ also seems to be dependent on distance. The dependence may be described as $\tau_{0.9}$ = 3.64 $R^{0.37}$ or $\log_{10}$ $\tau_{0.9}$ = (0.5 ± 0.043) + (0.41 ± 0.023) $\log_{10} R$. The com-

parison between empirical PGA values and those calculated using the average-soil spectral model (magnitude range 6.5 $< M_L <$ 7.0) is shown in Figure 16b. In this case, the initial model was changed. We multiplied the modeled spectra by the frequency-dependent coefficients (see Fig. 6f) reflecting the shallow-earthquake effect. Frequency-dependent attenuation of spectral amplitudes was described by $Q(f) = 80f^{0.8}$. The average value of residuals between the observed data and modeled, using the mean spectra, PGAs (model bias) is about -0.03, and standard deviation of residuals is about 0.21 log unit (Fig. 16c).

Response Spectra. The comparison between empirical and modeled 5% damped response spectra is shown in Figure 17 in the form of distribution of amplitudes at certain frequencies versus distance. Figure 18 shows comparison of the averaged empirical spectra and modeled ones. For the mainshock, the empirical spectra at distances 45–55 km were taken from the eastern and southern directions from the earthquake source, to avoid the influence of surface waves across Western Coastal Plain (see also Fig. 8, 9). In this case, when calculating the response spectra, no filtration below 0.4 Hz was applied. The modeled spectra were evaluated from the synthetic acceleration time functions (average values). Again, when predicting the response spectra, we use the mean average-soil Fourier spectra, mean plus one and mean plus two standard deviation values. It is seen that the modeled response spectra show a good agreement with the empirical spectra in the whole frequency range considered (0.3–10 Hz).

Discussion and Conclusion

The Chi-Chi, Taiwan, earthquake and aftershocks produced a rich set of strong ground-motion recordings, and the data have been already studied by several authors. The analyses of the peak ground acceleration values showed (EERI, 1999; Tsai and Huang, 2000; Boore, 2001) that, when considering the distribution of ground-motion parameters versus closest distance to the surface rupture (Chelungpu fault), the overall level of the observed horizontal PGAs from the earthquake is about 50% below the median PGA based on commonly used attenuation in California for M_w 7.6–7.7 (Boore *et al.*, 1997; Campbell, 1997; Sadigh *et al.*, 1997). The Chi-Chi PGA values are equivalent to what would be predicted for M_w 6.6, 6.0, and 6.2 from the attenuation models of Campbell, Boore *et al.*, and Sadigh *et al.* respectively (Tsai and Huang, 2000). Unlike the horizontal PGA, the peak ground velocity (PGV) values are relatively high (about 80% higher) compared to those predicted by existing PGV attenuation model (Campbell, 1997). Therefore, the Chi-Chi earthquake was called a high-velocity (HV)–low acceleration (LA) earthquake (high-PGV, low-PGA). On the other hand, however, the phenomenon is a result of excitation of the weak Chelungpu fault and sliding of sediments along the fault during a pure thrust earthquake. On the other hand, the long-period velocity waveforms observed at western direction from the Chelungpu fault (footwall) may be explained (e.g., Furumura *et al.*, 2000) by generation of surface waves at the deep alluvium plain area (the Western Coastal Plain). The PGA studies revealed also a strong basin response on the mainshock in the Taipei area (Tsai and Huang, 2000; Tsai *et al.*, 2000; Fletcher, 2001) and Ilan plain (Liu and Wen, 2000). The peculiarities of near-fault ground motions, including the response spectra, were analyzed by Loh *et al.* (2000), Somerville (2000), and Tsai and Huang (2000). Obviously, the numerous data from the Chi-Chi earthquake will be further studied regarding various areas in earthquake science.

Every disastrous earthquake produces a set of questions, and one of the major questions is, why was the damage so extensive? There are two reasons for damage during earthquakes: (a) underestimation of seismic loading that leads to an improper design and (b) quality of construction. In engineering practice, seismic loads are evaluated from zonation maps that are constructed on the basis of seismic hazard analysis. The assessment of seismic hazard, in turn, is performed using information on parameters of seismic source zones (configuration, maximum magnitudes, etc.), seismicity (earthquake recurrence), and ground-motion attenuation relationships. We are not going to discuss here the question of why the area where the Chi-Chi earthquake occurred was considered a zone with relatively low, for Taiwan, seismic potential (Building Technology Standards, 1997; Tsai et al., 2000). Here, we deal with the other type of uncertainties in seismic hazard analysis: the uncertainty connected with the ground motion during some future earthquake. The regional empirical model for average-soil Fourier amplitude spectra of ground acceleration was developed recently using the Taiwan database from small and moderate earthquakes ($5.0 < M_L < 6.5$) (Sokolov *et al.*, 1999, 2000). Thus, we attempted to answer the question, how well do the available ground motion models predict the observed Chi-Chi motions? Recalling that the spectral model is based on local magnitude (M_L) values, and bearing in mind the difference between the reported M_L and M_W values for the mainshock and aftershocks (see Table 1), the problem of applicability of local magnitude is also analyzed, at least for large thrust earthquakes in the Taiwan region.

The comparison of the ground-motion data collected during the M_L 7.3 Chi-Chi earthquake and large aftershocks allows us to make an affirmative answer to our questions. The application of spectral model, which was evaluated for the correspondent larger interval of local magnitude from the smaller magnitudes data, exhibits a good agreement with the observations (Fourier amplitude spectra, peak ground acceleration, and response spectra) from deep aftershock EQ92106 (M_L 6.8, depth 15 km, reverse faulting). The analysis of observed data from shallow aftershock EQ92107 (M_L 6.8, depth 10 km, reverse faulting) revealed the necessity to revise the parameters of spectral attenuation (Q-model) and to introduce empirical frequency-dependent coefficients (the

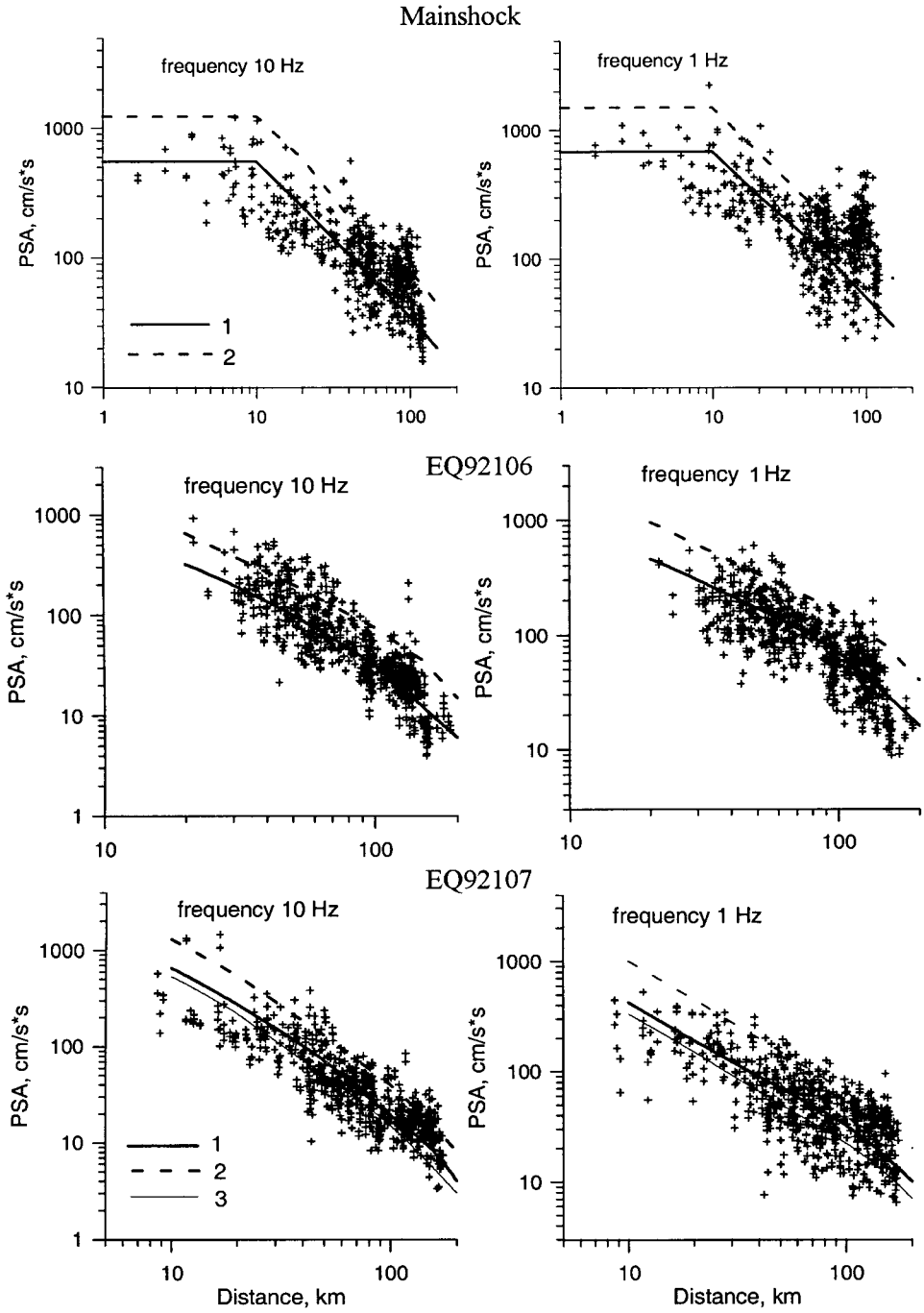

Figure 17. Comparison between the values of observed 5% damped response spectra (symbols) and the response spectra modeled using average-soil Fourier acceleration spectra (lines). The solid line (1) shows the spectra calculated using the mean values of the model; the dashed line (2) shows mean + 1 standard deviation. For aftershock EQ92107 the thin solid line (3) shows values calculated using the model without consideration of any shallow earthquake effect (see Fig. 6f).

so-called shallow-earthquake effect) for better fitting of the modeled spectra with the observation. After the revision, the modeled ground motion parameters also exhibit a good agreement with the observations; however, the observed Fourier acceleration spectra for the very shallow aftershock EQ92102 (M_L 6.6, depth 3.5 km, strike-slip faulting), which occurred 16 minutes later the mainshock, reveal a large discrepancy, both in shape and amplitude, with the modeled spectra.

The Q-factor is an important parameter of the ground-

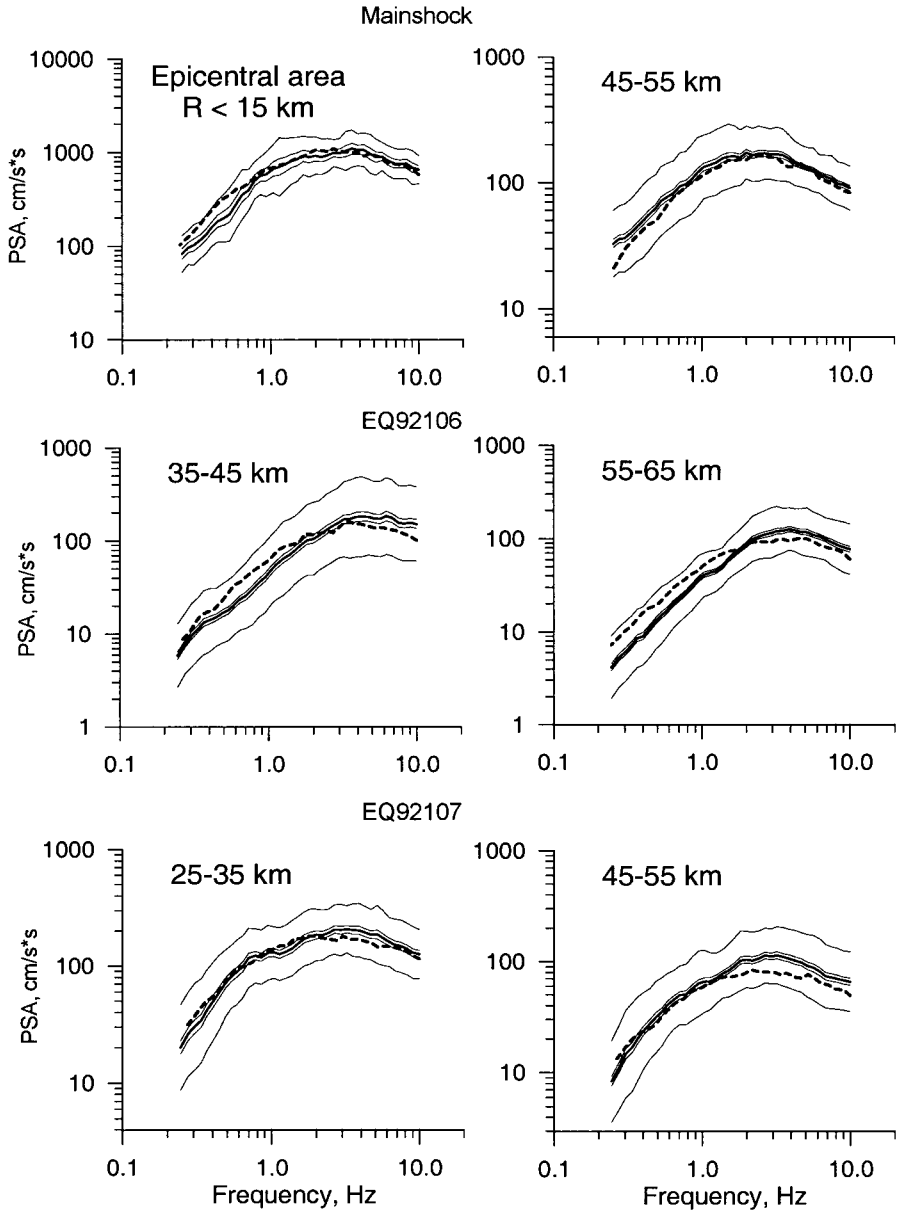

Figure 18. Comparison between observed response spectra (solid lines show the mean values and mean ± 1 standard deviation for a certain interval of distance), and predicted, using average-soil model (dashed lines), spectra for the mainshock and two aftershocks.

motion model; it depends on the wave-transmission quality of rock in the region. Numerous determination of the Q-values throughout the world (e.g., Aki, 1980; see also Lam *et al.*, 2000, for a recent review) showed that they are generally higher for the harder (older) rocks in the stable regions (for example, $Q_0 = 680–1100$ for eastern North America) and lower for the softer (young) rocks or tectonically active regions (for example, $Q_0 = 200$ for California, or $Q_0 = 100$ for southeastern Australia). The averaged value of Q_0 for the mountain areas is about 90 (Aki, 1987). We showed recently (Sokolov *et al.*, 1999, 2000) that, for the Taiwan region, the Q-factor depends on earthquake depth and Q_0 varies from 220 for deep earthquakes (depth more 35 km) to 125 for earthquakes with depth less than 35 km. These values are close to those determined in previous analyses (Wang, 1993). In this study, on the basis of large amount of additional empirical data the Q-factor has been found to be equal 80 for very shallow earthquakes with hypocentral depth less than 10 km. Obviously, the variations reflect the properties of the Earth's crust in the tectonically active Taiwan region.

The ground-motion data from the large and complex Chi-Chi earthquake are characterized by several peculiarities, which may be described by a joint influence of the effects of rupture propagation along the fault plane, shallow

crustal structure, and subsurface geological condition (e.g., Furumura *et al.*, 2000; Huang and Chen, 2000; Liu and Wen, 2000; Somerville, 2000; Tsai and Huang, 2000; Fletcher, 2001). These peculiarities include the movement of sediments along the ruptured Chelungpu fault, the long-period waveforms in deep alluvium plain area (the Western Coastal Plain), the ground motion enhancing to the north from the source at epicentral distances around 80 and 120 km at frequency range less than 1 Hz, and the response of the deep basin. When the ground motions are not affected by these phenomena (i.e., epicentral zone, eastern, and southern direction from the source at distances up to 80–90 km), however, the modeled average-soil spectra for magnitude range $7.0 < M_L < 7.5$ exhibit a good agreement with the observed spectra at frequencies greater than 0.2 Hz. For distances less than 40–50 km, the modeled spectra also almost exactly fit the observed spectra from the WCP area (west of the source) at frequencies more than 0.8–0.9 Hz, where the influence of surface waves is negligible. For the case of northern spectra at distances more than 50 km, the observed spectra are higher than the modeled ones and the difference increases with distance. When the average-soil spectral model and a stochastic technique were applied for evaluation of PGA values and response spectra, the comparison of observed and modeled data also showed a good agreement, at least for the eastern and southern data. In all the cases considered, the ground-motion parameters predicted using mean plus 1 standard deviation spectra provide a reliable upper limit for the observations. The predictions based on the mean plus 2 standard deviation spectra also overlap the effect of the Taipei basin response on the mainshock (northern data, distances 90–110 km).

Of course, the observed ground motions are characterized by certain peculiarities and they do, to a some extent, differ from the model. In general, however, it is possible to conclude that the local magnitude-based average-soil spectral model, which was recently developed for the Taiwan region, may be applied for prediction of spectral amplitudes (within frequency range 0.3–12 Hz) and peak ground acceleration for larger reverse-fault earthquakes. The next statement can be directly inferred: the Chi-Chi earthquake and at least two large aftershocks (EQ92106 and EQ92107) should be considered as typical events for the Taiwan region. The overall level of ground motions at short and intermediate periods (from 0.1–3.0 sec) is not surprisingly weak. Quite the contrary, it follows the regional source scaling relations. The only surprising phenomenon of the earthquake is that the short-period ground motions in the region cannot be described by the attenuation models developed for California, which are based on moment magnitude values and were derived for strike-slip events; however, it is widely accepted that attenuation may be different for different seismic regions and that it is necessary to construct region-specific ground motion models. The recently developed approach (coefficients β_M) for evaluation of ground motion spectra on the basis of data from smaller earthquakes in the studied region has been found capable of providing reliable results in the case of Taiwan region and the Chi-Chi earthquake.

The revised spectral model obtained in this study may be considered as a basis for subsequent analyses of peculiarities of the Chi-Chi earthquake strong ground motion in the near-field zone, including the finite-fault effect and nonlinear soil response. At the same time, it is possible to study the response of sediment-filled basins (for example, the Taipei basin, TAP array) on earthquakes of various magnitudes, distances, and location (including the Chi-Chi earthquake and aftershocks). These are the tasks of future research.

Acknowledgments

The authors would like to thank David Boore for thoughtful review comments and suggestions, which significantly helped improve the earliest version of the article. The constructive comments from Yoshimitsu Fukushima, Hiroshi Kawase, and anonymous reviewer are gratefully acknowledged. Ground-motion records of the Chi-Chi earthquake sequence were provided by the National Weather Bureau of the Republic of China. The study was supported by the National Science Council of the Republic of China under Grant Number NSC89-2811-E-319-0005.

References

Aki, K. (1980). Scattering and attenuation of shear waves in the lithosphere, *J. Geophys. Res.* **85,** 6496–6504.

Aki, K. (1987). Strong motion seismology, in *Strong Ground Motion Seismology*, M. O. Erdik and M. N. Toksöz, (Editors), NATO ASI Series C. Mathematical and Physical Sciences, Vol. 204 Dordrecht, Boston, 3–40.

Anderson, J., and S. Hough (1984). A model for the shape of the Fourier amplitude spectrum of acceleration at high frequencies, *Bull. Seism. Soc. Am.* **74,** 1969–1993.

Arefiev, S. S. (1985). Gradation of spectra from near earthquakes, in *Macroseismic and Instrumental Studies of Strong Earthquakes* Problems of Engineering Seismology, 26, Nauka, Moscow 134–141 (in Russian).

Atkinson, G. M. (1993). Earthquake source spectra in Eastern North America, *Bull. Seism. Soc. Am.* **83,** 1778–1798.

Atkinson, G. M., and D. M. Boore (1995). Ground-motion relations for eastern North America, *Bull. Seism. Soc. Am.* **85,** 17–30.

Atkinson, G. M., and W. Silva (1997). An empirical study of earthquake source spectra for California earthquakes, *Bull. Seism. Soc. Am.* **87,** 97–113.

Atkinson, G. M., and W. Silva (2000). Stochastic modeling of California ground motions, *Bull. Seism. Soc. Am.* **90,** 255–274.

Boore, D. M. (1983). Stochastic simulation of high frequency ground motion based on seismological model of the radiated spectra, *Bull. Seism. Soc. Am.* **73,** 1865–1894.

Boore, D. M. (2001). Comparison of ground motions from the 1999 Chi-Chi earthquake with empirical predictions largely based on data from California, *Bull. Seism. Soc. Am.* **91,** 1212–1217.

Boore, D. M., and G. M. Atkinson (1987). Stochastic prediction of ground motion and spectral response parameters at rock sites in eastern North America, *Bull. Seism. Soc. Am.* **77,** 440–467.

Boore, D. M., and W. B. Joyner (1997). Site amplification for generic rock sites, *Bull. Seism. Soc. Am.* **87,** 327–341.

Boore, D. M., W. B. Joyner, and T. E. Fumal (1997). Equations for estimating horizontal response spectra and peak acceleration from western north American earthquakes: a summary of recent work, *Seism. Res. Lett.* **68,** 128–153.

Building Technology Standards (1997), Ministry of Interior, Taipei, Taiwan, R.O.C.

Campbell, K. W. (1997). Empirical near-source attenuation relationships for horizontal and vertical components of peak ground acceleration, peak ground velocity, and pseudo-absolute acceleration response spectra, *Seism. Res. Lett.* **68,** 154–179.

Chang, T.Y., J. Anglier, F. Cotton, and T. C. Shin (2000). Determination of seismic attenuation laws based on analyses of peak ground acceleration in Taiwan, in *Proc. of International Workshop on Annual Commemoration of Chi-Chi Earthquake*, 18–20 September 2000, National Center for Research on Earthquake Engineering, Taipei, Taiwan, Vol. 1, 251–262.

Cheng, S. N., Y. T. Yeh, C. H. Loh, C. H. Chang, and T. C. Shin (2000), Strong-motion data reduction for aftershocks of Chi-Chi earthquake, in *Proc. of International Workshop on Annual Commemoration of Chi-Chi Earthquake*, 18–20 September 2000, National Center for Research on Earthquake Engineering, Taipei, Taiwan, Vol. 1, 275–282.

Chernov, Yu. K. (1984). Relationships for ground motion spectra in near-field zone, in *Prediction of Seismic Effect*, Nauka, Moscow, 16–28 (in Russian).

Chernov, Yu. K. (1989). *Strong Ground Motion and Quantitative Assessment of Seismic Hazard*, Fan Publishing House, Tashkent (in Russian).

Earthquake Engineering Research Institute (1999). The Chi-Chi Taiwan earthquake of September 21, 1999, EERI Special Earthquake Report, EERI, Oakland, California.

Fletcher, J. B. (2001). Ground motion in the Taipei and Ilan basin, *Seism. Res. Lett.* **2,** 283.

Fukushima, Y. (1996). Scaling relations for strong ground motion prediction models with M^2 terms, *Bull. Seism. Soc. Am.* **86,** 329–336.

Furumura, T., K. Koketsu, K. L. Wen, and M. Furumura (2000). Numerical simulation of strong ground motion during the Chi-Chi, Taiwan, earthquake, in *Proc. of International Workshop on Annual Commemoration of Chi-Chi Earthquake*, 18–20 September 2000, National Center for Research on Earthquake Engineering, Taipei, Taiwan, Vol. 1, 222–232.

Gusev, A. (1983). Descriptive statistical model of earthquake source radiation and its application to an estimate of short-period strong motion, *Geophys. J. R. Astr. Soc.* **74,** 787–808.

Hanks, T. C., and R. K. McGuire (1981). The character of high-frequency strong ground motion, *Bull. Seism. Soc. Am.* **71,** 2071–2095.

Huang, C. T., and S. S. Chen (2000). Near-field characteristics and engineering implications of the 1999 Chi-Chi earthquake, *Earthq. Eng. Eng. Seism.* **2,** 23–41.

Irikura, K, K. Kamae, and L. A. Dalguer (2000). Source model for simulating ground motion during the 1999 Chi-Chi earthquake, in *Proc. of International Workshop on Annual Commemoration of Chi-Chi Earthquake*, 18–20 September 2000, National Center for Research on Earthquake Engineering, Taipei, Taiwan, Vol. 1, 1–12.

Iwata, T., H. Sekiguchi, and K. Irikura (2000), Rupture process of the 1999 Chi-Chi, Taiwan, earthquake and its near-source strong ground motions, in *Proc. of International Workshop on Annual Commemoration of Chi-Chi Earthquake*, 18–20 September 2000, National Center for Research on Earthquake Engineering, Taipei, Taiwan, Vol. 1, 36–46.

Khalturin, V. I., T. G. Rautian, and A. Nurmagambetov (1975). Dependence of seismic motion spectra on earthquake energy, in *Quantification Problem of Seismic Hazard*, Nauka, Moscow, p. 123–139 (in Russian).

Koyama, J., and S.-H. Zheng (1985). Excitation of short-period body-waves by great earthquakes, *Phys. Earth Planet. Inter.* **37,** 108–123.

Lam, N, J. Wilson, and G. Hutchinson (2000). Generation of synthetic earthquake accelerograms using seismological modelling: a review, *J. Earthq. Eng.*, **4,** 321–354.

Lee, C. T., K. I. Kelson, and K. H. Kang (2000). Hanging-wall deformation and its effect to building and structures as learned from the Chelungpu faulting in the 1999 Chi-Chi, Taiwan earthquake, in *Proc. of International Workshop on Annual Commemoration of Chi-Chi Earthquake*, 18–20 September 2000, National Center for Research in Earthquake Engineering, Taipei, Taiwan, Vol. 1, 93–104.

Lee, C. T., C. T. Cheng, C. W. Liao, and Y. B. Tsai (2001). Site classification of Taiwan free-field strong-motion stations, *Bull. Seism. Soc. Am.* **91,** 1283–1297.

Lee, S. J., and K. F. Ma (2000). Rupture process of the 1999 Chi-Chi, Taiwan, earthquake from the inversion of teleseismic data, *Terr. Atmos. Ocean Sci.*, **11,** 591–608.

Liu, L. F., and K. L. Wen (2000). The site response of Lanyang basin on the Chi-Chi earthquake sequence, in *Proc. of International Workshop on Annual Commemoration of Chi-Chi earthquake*, 18–20 September 2000, Taipei, Taiwan, Vol. 1, 294–304.

Loh, C.-H., Z.-K. Lee, T.-C. Wu, and S.-Y. Peng (2000). Ground motion characteristics of the Chi-Chi earthquake of 21 September 1999, *J. Earthq. Eng. Struct. Dyn.* **29,** 867–897.

Sadigh, K., C.-Y. Chang, J. A. Egan, F. Makdisi, and R. R. Youngs (1997). Attenuation relationships for shallow crustal earthquakes based on California strong-motion data. *Seism. Res. Lett.* **68,** 180–189.

Shin T.-C., K.-W. Kuo, W. H. K. Lee, T.-L. Teng, and Y.-B. Tsai (2000). A preliminary report on the 1999 Chi-Chi (Taiwan) earthquake, *Seism. Res. Lett.* **71,** no. 3, 24–30.

Sokolov, V. Yu. (1998). Ground acceleration spectra from Caucasus earthquakes, *Izvestiya, Phys. Solid Earth* **34,** 663–675.

Sokolov, V. Yu. (2000a). Hazard-consistent ground motions: generation on the basis of uniform hazard Fourier spectra, *Bull. Seism. Soc. Am.* **90,** 1010–1027.

Sokolov, V. Yu. (2000b). Macroseismic intensity as a function of Fourier amplitude spectra: a tool to evaluate the regional and local peculiarities of the intensity distribution. *Proc. of XXVII General Assembly of the European Seismological Commission*, Lisbon, 10–15 September 373–377.

Sokolov, V. Yu., and Yu. K. Chernov (1998). On the correlation of seismic intensity with Fourier acceleration spectra, *Earthq. Spectra*, **14,** 679–694.

Sokolov, V. Yu., and Yu. K. Chernov (2001). Probabilistic microzonation of the urban territories, *Pure Appl. Geophys.* **158,** 2295–2312.

Sokolov, V. Yu., C.-H. Loh, and K.-L. Wen (1999). Empirical models for estimating design input ground motions in Taiwan region, in *Proc. of International Workshop on Mitigation of Seismic Effects on Transportation Structures*, 12–14 July 1999, Taipei, Taiwan, 154–163.

Sokolov, V. Yu., C.-H. Loh, and K.-L. Wen (2000). Empirical model for estimating Fourier amplitude spectra of ground acceleration in Taiwan region, *J. Earthq. Eng. Struct. Dyn.* **29,** 339–357.

Sokolov, V. Yu, C. H. Loh, and K. L. Wen (2001a). Empirical models for site and region-dependent ground-motion parameters in Taipei area: a unified approach. *Earthq. Spectra* **17,** 313–331.

Sokolov, V. Yu., C. H. Loh, and K. L. Wen (2001b). Site-dependent input ground motion estimations for the Taipei area: a probabilistic approach, *Probabilistic Eng. Mech.* **16,** 177–191.

Somerville, P. G. (2000). Magnitude scaling of near fault ground motions, in: *Proc. of International Workshop on Annual Commemoration of Chi-Chi earthquake*, 18–20 September, Taipei, Taiwan, Vol. 1, 59–70.

Trifunac, M. D., and A. G. Brady (1975). A study of the duration of strong earthquake ground motion, *Bull. Seism. Soc. Am.* **65,** 581–626.

Tsai, K. C, C. P. Hsiao, and M. Bruneau (2000). Overview of building damages in 921 Chi-Chi earthquake, *Earthq. Eng. Eng. Seismol.* **2,** 93–108.

Tsai, Y. B., and M. W. Huang (2000). Strong ground motion characteristics of the Chi-Chi, Taiwan earthquake of September 21, 1999, *Earthq. Eng. Eng. Seismol.*, **2,** 1–21.

Wang, J. H. (1993). Q values of Taiwan: a review. *J. Geol. Soc. China*, **36,** 15–24.

Wang, C. Y., C. H. Chang, and H. Y. Yen (2000). An interpretation of the 1999 Chi-Chi earthquake in Taiwan based on thin-skinned thrust model, *Terr., Atmos. Ocean Sci.* **11,** 609–630.

Wen, K.-L., and Y.-T. Yeh (1991). Characteristics of strong motion durations in the SMART1 array area, *Terr., Atmos. Ocean Sci.* **2,** 187–201.

Wen, K.-L., and Y.-C. Yeh (2001). Nonlinear soil response during the 1999 Chi-Chi, Taiwan earthquake, *Seism. Res. Lett.* **72,** 248.

Yagi, Y., and M. Kikuchi (2000). Source rupture process of the Chi-Chi, Taiwan earthquake determined by seismic waves and GPS data (abstract), *Eos Trans. Am. Geophys. Union* **81,** no. 22, S21A-05.

Geophysical Institute of Karlsruhe University,
Hertzstr. 16
76187 Karlsruhe
Germany
Vladimir_Sokolov@gpi.uni-karlsruhe.de
(V.Yu.S.)

National Center for Research on Earthquake Engineering
200, Sec. 3
Hsinhai Rd.
Taipei 106
Taiwan, R.O.C.
lohc@ncree.gov.tw
(C.-H.L.)

Institute of Applied Geology
National Central University
Chung Li, Taoyuan County
Taiwan 32054, R.O.C.
wenkl@eqm.gep.ncu.edu.tw
(K.-L.W.)

Manuscript received 31 May 2001.